Isr. J. Earth Sci.; 55: 69–93

Four successive episodes of Late Pan-African dikes in the central Elat area, southern Israel

Yaron Katzir,[a] Boris Litvinovsky,[a,b] Moshe Eyal,[a] Ada Zanvilevich,[a] and Yevgeny Vapnik[a]
[a]Department of Geological and Environmental Sciences, Ben-Gurion University of Negev, P.O. Box 653, Be'er Sheva 84105, Israel
[b]Geological Institute, Siberian Division of the Russian Academy of Sciences, Ulan-Ude, Russia

(Received 2 October 2005; accepted in revised form 12 December 2006)

ABSTRACT

Katzir, Y., Litvinovsky, B., Eyal, M., Zanvilevich, A., and Vapnik, Y. 2006. Four successive episodes of Late Pan-African dikes in the central Elat area, southern Israel. Isr. J. Earth Sci. 55: 69–93.

Four successive Late Pan-African dike suites are recognized in the central Elat area: (1) microdiorite and lamprophyre; (2) dacite porphyry with subordinate andesite and feldspathic (Fsp) rhyolite porphyry; (3) quartz porphyry and Fsp-rhyolite porphyry with minor trachydolerite and trachyandesite; (4) trachydolerite, mostly high-Ti. Dike swarms formed over the period of ~600 Ma to 530 Ma. The dike episodes alternated with plutonic, volcanic, and sedimentary events. Microdiorite and lamprophyre from suite 1 correspond to calc-alkaline, medium- to high-K trachyandesite. Dacite porphyry is prevalent in suite 2 and forms together with augite-bearing andesite and rhyolite a high-K calc-alkaline series. In suite 3 silicic rocks are dominant; they are alkaline (NK/A >0.9) and have chemical characteristics of A-type granites. Among the trachydolerites from suites 3 and 4, high-Ti varieties are abundant (2.8–2.9 wt% and 3.3–4.5 wt% TiO_2, respectively). Trachydolerites are enriched in REE, Zr, Y, Ti, and P.

Although Late Pan-African dikes are postorogenic, magmas of the first two suites were derived from mantle sources that are characteristic of a subduction-related environment of active continental margins. Trachydolerites-3 and -4 were produced, however, from sources enriched in asthenospheric components. Late Pan-African dike swarms similar to those described in southern Israel are extremely abundant throughout the Sinai Peninsula and Eastern Desert of Egypt. Significant overlap of compositions in mafic dike rocks from southern Israel and the same rock types from southern Sinai suggest similar sequence and sources of dikes over a large region.

INTRODUCTION

Southern Israel, the Sinai Peninsula, and the adjacent basement outcrops of southwestern Jordan, comprise the northernmost part of the Arabian–Nubian Shield (ANS). The evolution of the ANS was accomplished in four main stages (Gass, 1982; Roobol et al., 1983; Bentor, 1985; Stern and Hedge, 1985; Kröner et al., 1987; Stern et al., 1988; Greiling et al., 1994; Garfunkel, 1999; Genna et al., 2002). During the *first and second stages* (~900–650 Ma) oceanic and island arc crust was created. At the end of the second stage, the

E-mail: ykatzir@bgu.ac.il

0021-2164/06 $4.00

oceanic and island arc terrains were amalgamated and accreted to form the ANS. The post-collision *batholithic stage* III (~650–600 Ma) marks stabilization of the shield and is characterized by widespread calc-alkaline magmatism, mainly of intermediate to acid composition. At the boundary between stages III and IV a fundamental transition in tectonic and magmatic style, from compressional to extensional, took place (Stern and Hedge, 1985; Garfunkel, 1999). The *fourth stage* (~600–530 Ma) involves formation of mainly alkaline to peralkaline granites and rhyolites, representing post-orogenic and within-plate magmatism. During the fourth (Late Pan-African) stage, widespread dike injection occurred throughout the whole territory of the ANS (Bentor and Eyal, 1987; Eyal and Eyal, 1987; Stern et al., 1988; Baer et al., 1993; Eyal et al., 1995; El-Metwally, 1997; Stein et al., 1997; Gutkin and Eyal, 1998; Iacumin et al., 1998; Kessel et al., 1998; Voznesensky, 1998; Essawy and El-Metwally, 1999; Genna et al., 2002). Dikes are concentrated in 20–40-km-wide swarms that can be followed intermittently for several tens of kilometers. The density of dikes is unusually high: on average, dikes cover 10% of the exposed area, although within some areas dikes may form >50% of all rocks (e.g., Eyal and Eyal, 1987; Gutkin and Eyal, 1998). Dike composition varies widely, from basalt to andesite to calc-alkaline and alkaline rhyolites.

It has long been established that the formation of Late Pan-African dike swarms in the Sinai Peninsula and adjacent territories occurred in several episodes. However, the number and sequence of episodes remain debatable. In the early compilation of Eyal and Eyal (1987), two episodes of late (unmetamorphosed) dike formation were recognized, but studies performed in the Sinai Peninsula during the last decade have demonstrated that the sequence of dike injections was more complex. The relative geochronological sequence of dikes is variable in different areas, but in most cases it is given, from older to younger, as acid, intermediate-basic, lamprophyre, bimodal basalt-rhyolite, and alkaline basalt (Stern and Gottfried, 1986; Stern and Manton, 1987; Friz-Töpfer, 1991; Iacumin et al., 1998; Abu-El-Ela and Salem, 1999; Essawy and El-Metwally, 1999).

In southern Israel almost all the main types of dikes that are characteristic of the northern part of the ANS are recognized (Bentor and Eyal, 1987; Eyal and Eyal, 1987). Several dike swarms extend from the Sinai Peninsula to southern Israel (Voznesensky, 1998). A number of dike episodes are distinguished in the Elat and Timna areas. However, data on the sequence of episodes are ambiguous. Garfunkel (1999) considers that, although some dikes predate young alkaline granite plutons, the most voluminous dike episode that can be divided into several stages took place after the formation of the alkaline Yehoshafat granite, but before the deposition of a volcano–conglomeratic series (Elat conglomerate, alkaline rhyolite, andesite). On the other hand, it was demonstrated that a large swarm of quartz porphyry dikes intersects the Elat conglomerate (Gutkin and Eyal, 1998) and the rhyolite volcanic suite (Mushkin et al., 1999, 2003). Stein, Navon, and Kessel (Kessel, 1995; Stein et al., 1997; Kessel et al., 1998) recognized three Late Pan-African dike suites: (1) calc-alkaline andesitic to rhyolitic; (2) basaltic to rhyolitic, mostly tholeiitic (TH1); and (3) tholeiitic (TH2), later called alkali-basalt suite.

In this paper, new data on the geology, petrography and chemical composition of the Late Pan-African dikes from the central Elat area, along with some considerations about probable magma sources, are presented.

GEOLOGICAL SETTING

General description

The study was performed in the central Elat area, the largest exposed outcrop of the Precambrian basement in southern Israel. Metamorphic and magmatic rocks in this block represent most stages of the evolution of the ANS (Fig. 1). Orthogneisses, metapelitic, and psammitic schists (Elat schist, Taba gneiss, Roded schist and gneiss, Elat granitic gneiss) were formed at the beginning of the island arc stage, within the time span of 800–740 Ma (Eyal et al., 1991). The Shahmon metagabbro dated to 640–650 Ma (Eyal et al., 1991) could be timed to the late island arc stage. Emplacement of the Roded quartz diorite and Shahmon gneissic granite occurred in the batholithic stage at 630–640 Ma (Katz et al., 1998; Eyal et al., 2004). At the late post-collision stage, the calc-alkaline peraluminous Elat granite (623 ± 24 Ma) formed a number of plutons (Eyal et al., 2004). Intracratonic magmatism is represented by the Yehoshafat alkaline granite (605 ± 4 Ma; Beeri, pers. comm.). The formation of shallow alkaline granite plutons was followed by fast uplift, extensive erosion, and differentiation of the area into basins and highs (Garfunkel, 1999). These processes were accompanied by molasse-like sedimentation represented by the Elat conglomerate and by volcanic activity.

Late Pan-African (unmetamorphosed) dikes of various sizes and compositions are abundant, although unevenly distributed, throughout the study area. The

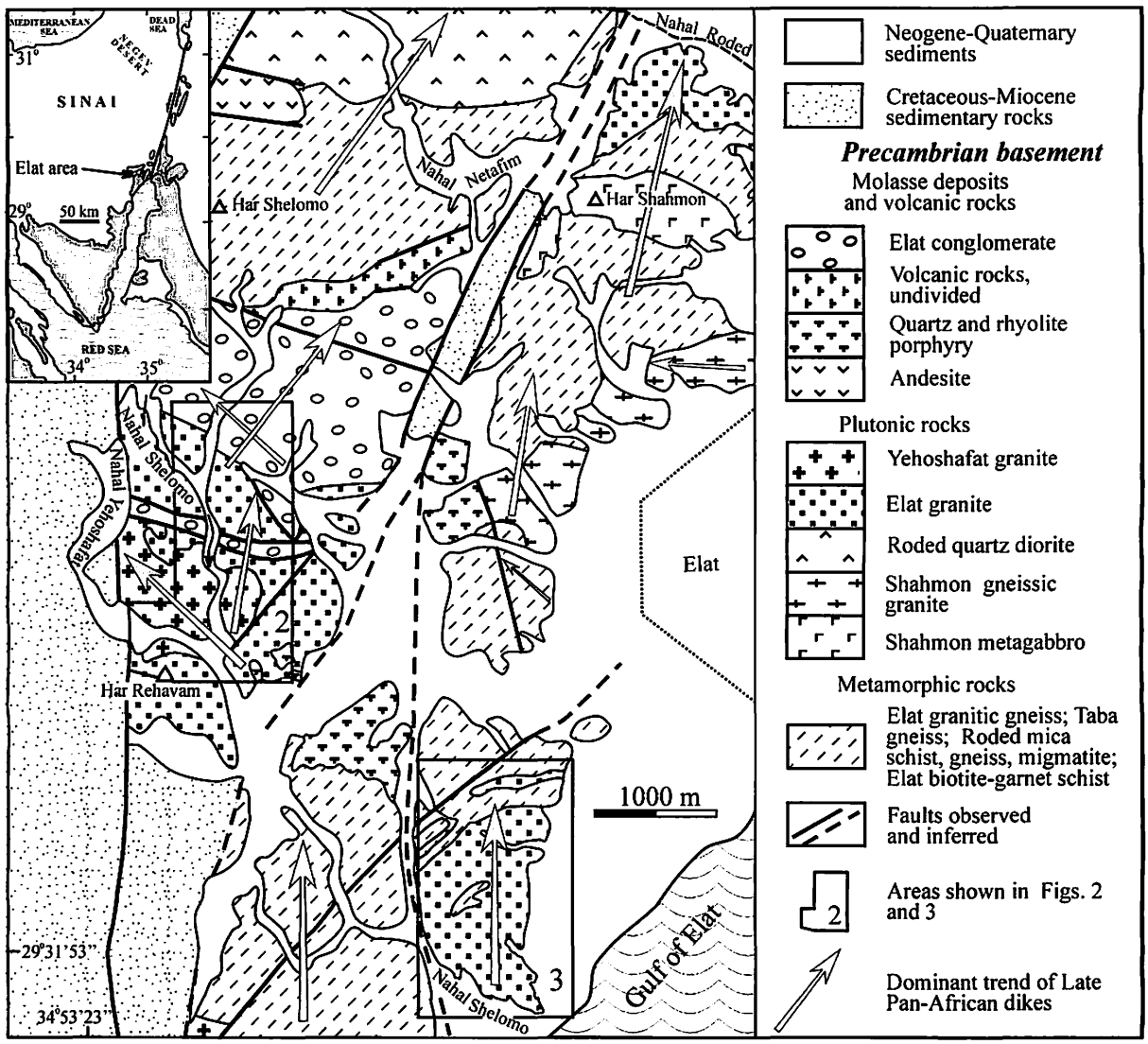

Fig. 1. Simplified geological map of the central Elat area (after Drukman et al., 1993 and Garfunkel et al., 2000, with modifications after Eyal et al., 2004).

highest concentrations of dikes are observed in the western part of the area and within the Nahal Shelomo pluton composed of the Elat granite (Figs. 2,3). In places, about 100 subparallel dikes can be counted within a 500–600-m-wide zone. In these zones, the proportion of country rock constitutes only 5–10% of the total rock volume and dikes commonly border one another (Fig. 2, inset A; Fig. 4). In the vicinity of Mt. Shelomo, within an area of about 2 km by 1 km, the proportion of dikes exceeds 50% and in places attains 80–90% (Gutkin and Eyal, 1998). Most of the dikes are vertical or steeply dipping; they are several hundred meters to 2 km long, and their width ranges from several tens of centimeters to about 30 m. In some large dikes, en echelon segments, commonly 0.5–1 km long, can be distinguished.

Sequence of dike episodes

The sequence of dike episodes has been recognized on the basis of study of more than 150 dikes, their cross-cutting relations, and their field relations to country rocks of different ages. Four successive dike suites were distinguished: *suite 1*, microdiorite and lamprophyre (spessartite); *suite 2*, dacite porphyry with subordinate andesite and Fsp-rhyolite porphyry; *suite 3*, quartz porphyry and Fsp-rhyolite porphyry with

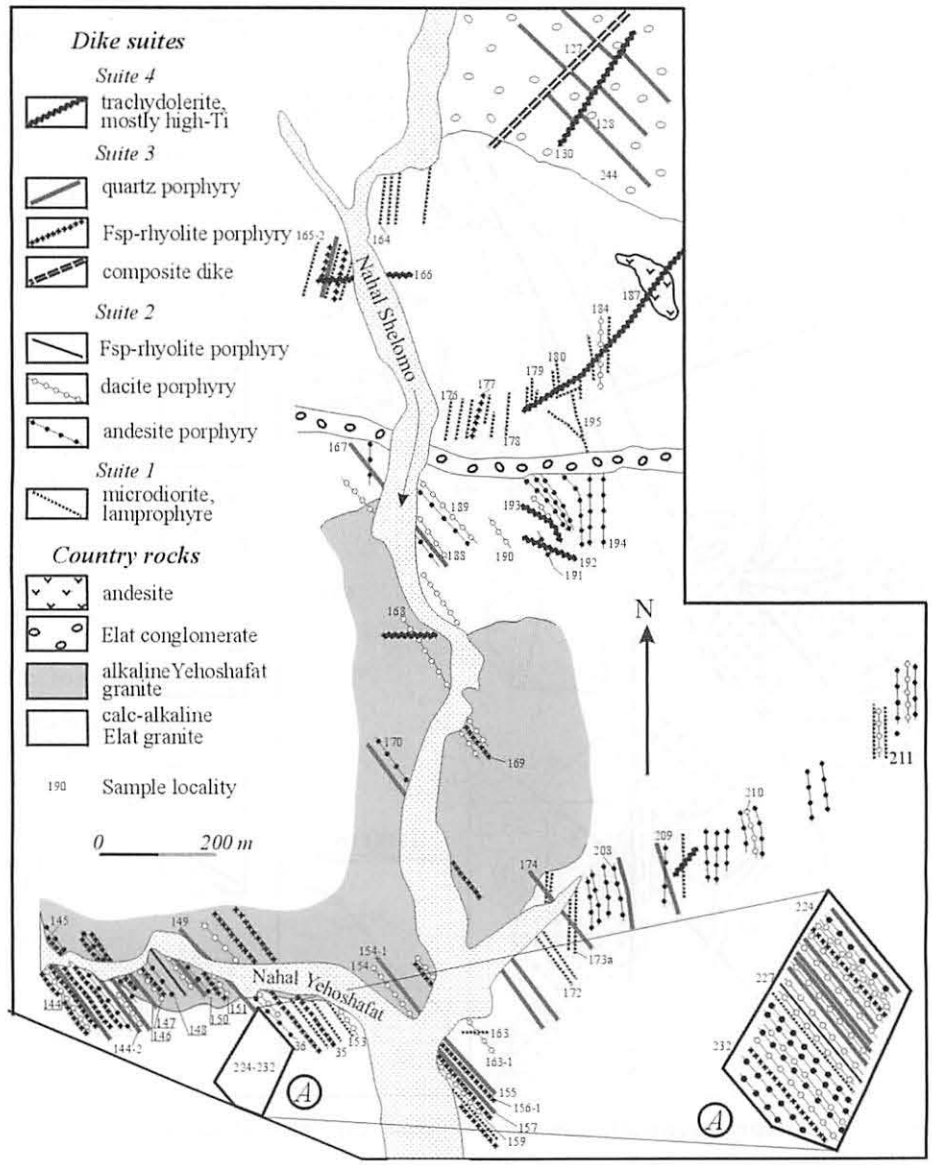

Fig. 2. Dikes from four successive suites in the Nahal Shelomo valley. Inset A illustrates 24 subparallel, steeply dipping dikes from different suites in a continuous 150-m-long outcrop. Dike thickness ranges from 2 to 15 m; most of the dikes border one another. Only the dikes that were found and studied in the course of the authors' field investigations are shown.

small proportions of trachydolerite and trachyandesite; *suite 4*, trachydolerite, mostly high-Ti.

The age of suite 1 is constrained by field relations in the lower reaches of the Nahal Yehoshafat valley (Fig. 4A; see Fig. 2, locality 35). Here, microdiorite dikes cut the Elat granite, but both granite and the dikes are intruded by the alkaline Yehoshafat granite that, in turn, is intersected by Fsp-rhyolite porphyry dikes from suite 3 and dacite porphyry from suite 2 (not shown in Fig. 4). Dikes of suite 2 are abundant in the Yehoshafat granite pluton (Fig. 2), but they do not cut the younger Elat conglomerate. Instead, in the northern part of the study area (Fig. 2, locality 244) two dikes of dacite porphyry that are characteristic only of suite 2 are overlain by the conglomerate. Numerous angular blocks of dacite porphyry occur within the conglomerate immediately near these dikes. Rhyolite porphyry and andesite porphyry cobbles and boulders up to 50 cm in diameter are also present in the conglomerate. The post-conglomerate age of suite 3 is clearly demonstrated by the abundance of quartz porphyry and, in places, mafic dikes that intersect the Elat

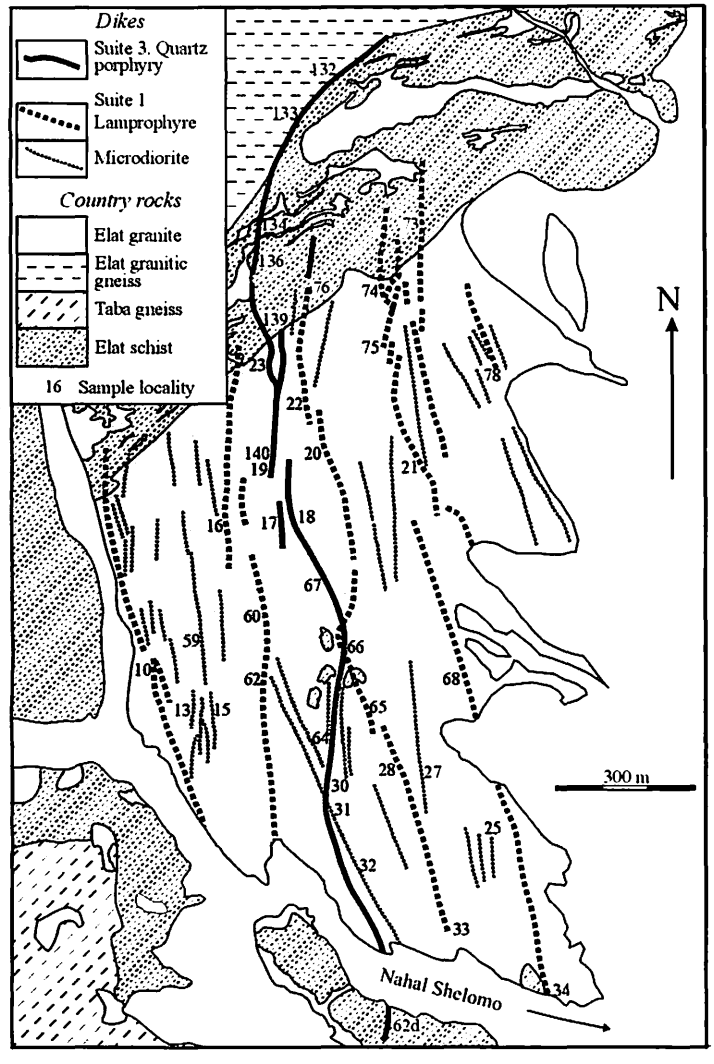

Fig. 3. Dikes from suites 1 and 3 in the Nahal Shelomo pluton.

Table 1
Correlation of Late Neoproterozoic dike episodes with plutonic, volcanic, and sedimentary events in southern Israel

Plutonic and volcanic activity, sedimentation	Dike suites
	4. Dolerite, mostly high-Ti, 531 ± 4.6 Ma[1]
	3. Quartz porphyry, feldspathic rhyolite porphyry, with small proportion of trachydolerite and trachyandesite, mostly in composite dikes
Trachyandesite and rhyolite volcanics, Elat conglomerate	
Uplift followed by extensive erosion, molasse sedimentation and volcanic activity	
	2. Dacite porphyry with subordinate andesite porphyry and feldspathic rhyolite porphyry
Yehoshafat alkaline granite, 605.4 ± 4 Ma[2]	
	1. Microdiorite and lamprophyre (spessartite)
Elat calc-alkaline peraluminous granite, 623 ± 24 Ma[3]	

Age data: [1]Beyth and Heimann, 1999. [2]Unpublished U–Pb zircon dating performed by Y. Beeri in the NORDSIM Facility, Swedish Museum of National History, Stockholm. [3]Eyal et al., 2004.

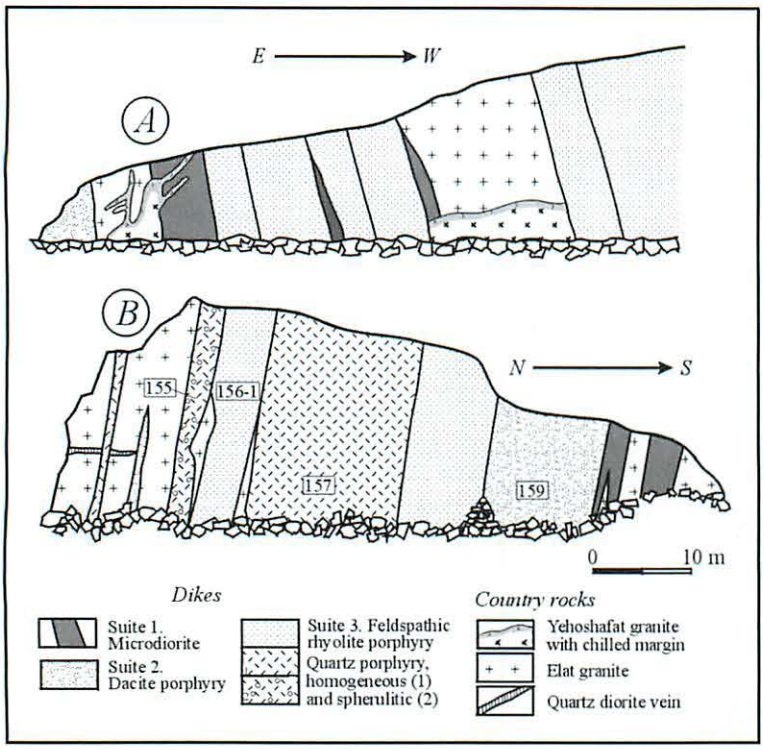

Fig. 4. Field relations between dikes and country rocks at the confluence of N. Shelomo and N. Yehoshafat. (A) The Yehoshafat alkaline granite intrudes both Elat granite and microdiorite dikes (suite 1); in turn, the Yehoshafat granite is intersected by feldspathic rhyolite porphyry dikes (suite 3). Lower reaches of Nahal Yehoshafat, see Fig. 2, locality 35. (B) Alternation of conformable steeply dipping dikes from suites 1, 2, and 3 at the eastern bank of the Nahal Shelomo valley (Fig. 2; localities 155–159). The chemical composition of the samples is given in Table 2.

conglomerate (Gutkin and Eyal, 1998; Fig. 2). Several quartz porphyry dikes and composite dikes that are typical of suite 3 crosscut alkaline rhyolite volcanics 10 km to the north, in the Amram block (Mushkin et al., 1999, 2003). Trachydolerites of suite 4 intrude the Elat conglomerate, a subvolcanic andesite body, and dikes of suite 3 (Fig. 2, localities 128 and 187).

The sequence of dikes and their temporal relations with sedimentary and magmatic rocks is presented in Table 1. It is noteworthy that dike episodes 1, 2, and 3 were divided in time by plutonic, volcanic, and sedimentation events.

Geology of dike suites

Suite 1 comprises two rock types, microdiorite and lamprophyre. The microdiorite dikes are smaller and homogeneous, whereas the lamprophyre dikes are infrequently more then 2 km long and their thickness varies from 6 to 12 m. A notable feature of the lamprophyre dikes is that in places they are inhomogeneous, with subordinate (≤ 5 vol%) finer-grained felsic rocks that occur as rounded and irregular patches, schlieren, and veins ranging in composition from quartz microdiorite to microgranite. The lamprophyre dikes are younger than the microdiorites (Fig. 3, locality 78). The two types are grouped into suite 1 since the lamprophyre and microdiorite dikes are closely spaced and were found only within the Elat granite and metamorphic rocks.

Suite 2 is composed of a spectrum of rock types, from andesite porphyry through dacite porphyry to Fsp-rhyolite porphyry with significant prevalence of dacitic rocks. Each rock type forms individual dikes, with crosscutting relations to one another. Interrelations between mafic and silicic rocks were studied in the Nahal Yehoshafat valley (Fig. 2). Although dikes are sub-parallel, oblique intersections and thin apophyses enable one to distinguish the order of injections, from earlier andesite porphyry to dacite porphyry to Fsp-rhyolite porphyry.

In *suite 3*, silicic rocks (quartz porphyry and subordinate Fsp-rhyolite porphyry) absolutely dominate over basic rocks: the proportion of trachydolerite and trachyandesite porphyry is about 5%. Silicic dikes are abundant throughout the Elat area (Fig. 5). Judging by the crosscutting relations, their emplacement occurred repeatedly. Several dikes are made up of ultrapotassic quartz porphyry with K_2O ranging from 6 to 10 wt% and Na_2O from 2 to 0.15 wt%. These rocks, as well as volcanic rhyolite of similar composition, are conventionally regarded as metasomatic (Agron and Bentor, 1981; Bentor, 1985; Wachendorf et al., 1985). Basic

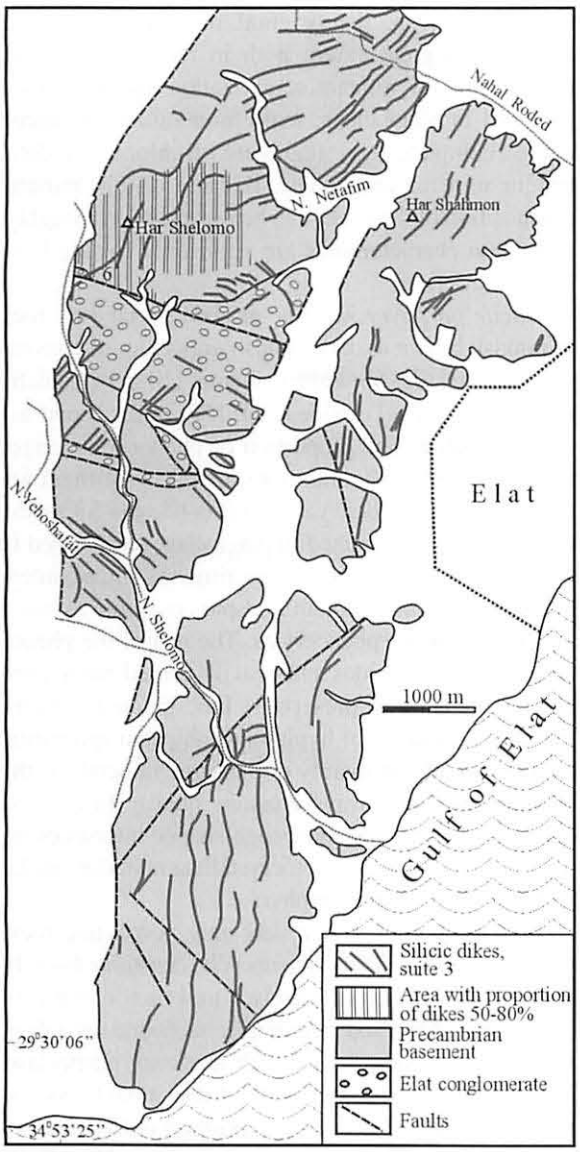

Fig. 5. Distribution of quartz porphyry and Fsp-rhyolite porphyry dikes from suite 3 in the Elat area (based on aerial photographs, interpretation by V. Voznesensky, with authors' supplements). The area with high proportion of dikes is shown after Gutkin and Eyal (1998).

rocks commonly form mafic margins in composite dikes whereas individual mafic dikes are rare. The composite dikes are referred to as dikes of the last phase of the suite 3 formation. In composite dikes the contact between mafic and felsic rocks is mostly planar and abrupt, but in some dikes it is gradational, with a 20–30-cm-wide zone of hybrid rocks produced by magma mixing.

The trachydolerite *dike suite 4* is poorly exhibited in the study area. Dolerite dikes strike in various directions (Fig. 2); they are scattered and heavily altered.

Correlation between the strike and age of dikes

Three main trends of dike swarms, N–S, N40–50°W, and N30–40°E, are dominant in the study area. Dikes of N–S direction are abundant in the eastern half of the Nahal Shelomo valley, whereas numerous NW-striking dikes occupy its western part (Fig. 2). Near the northern border of area 2 (Fig. 1) dikes striking NE are found along with dikes of NW direction (Fig. 2, locality 127). Further to the north the NE direction of dikes prevails (Fig. 5).

A previous study that focused on a smaller area within the Elat exposures argued that each dike suite is characterized by a different direction (Stein et al., 1997; Kessel et al., 1998). However, our extensive observations of the whole Elat area show that there is no simple correlation between the age and strike of the dikes. This is clearly demonstrated in the southwestern part of the Nahal Shelomo area. Dikes formed during three successive stages, from 1 to 3, strike N35°W (Figs. 2 and 4B). Submeridional trends of both microdiorite and lamprophyre dikes from suite 1 and an adjacent quartz porphyry dike from suite 3 are observed in the Nahal Shelomo pluton area, as well as in the upper reaches of the Nahal Shelomo valley (Figs. 2, 3). Crosscutting relations between younger and older dikes are clearly exhibited within a narrow zone wherein dike swarms of different directions overlap (the Nahal Shelomo valley, Fig. 2, localities 167, 174, and 209). Also we observed that some dikes within this zone change their direction (Fig. 2, locality 194): of six adjacent andesite porphyry dikes from suite 2, two dikes strike exactly to the north, three dikes strike N40°W, and one dike between these two groups strikes to the north, then turns to N40°W.

All the above data suggest that in the study area the stress field that controlled the dike swarm direction prevailed from the earliest dike injection episode and did not change markedly during the whole period of dike formation.

ANALYTICAL METHODS

Whole-rock chemical analyses were made using a combination of wet chemical methods, AAS, and titration (major elements), and X-ray fluorescence (Rb, Sr, Ba, Y, Zr, and Nb) at the Geological Institute, Siberian Division of the Russian Academy of Sciences, Ulan-Ude. Rare earth and some selected trace elements (Hf, Ta, Th, U, Ga, V, Cu, Pb, Zn, Sc, and Cs) were analyzed by the ICP-MS method at the Institute

of Mineralogy and Geochemistry of Rare Elements, Moscow, and in the National Taiwan University, Taipei. Analyses are considered accurate to within 2–5% for major elements, and better than 10–15% for trace elements. The accuracy for all the REE (except Lu) is 1–5%; for Lu, it is 9–10%.

Microprobe mineral analyses were carried out using a modernized four-channel MAR-3 electron probe microanalyzer at the Geological Institute, Ulan-Ude. Analyses were obtained with a beam of 2–3 μm diameter. Operating conditions were 20 kV, 40 μA beam current, and a counting time of 10 s. The detection limits are 0.05–0.09 wt% for Na_2O, MgO, Al_2O_3, and SiO_2; 0.01–0.05 wt% for K_2O, CaO, TiO_2, MnO, and FeO.

PETROGRAPHY

Suite 1. Microdiorite is dark greenish with a fine-grained matrix of pilotaxitic and prismatic granular texture. Phenocrysts commonly make up 8–10% of the rock volume; some dikes are almost aphyric, whereas in others the amount of phenocrysts reaches 50–55 vol%. Phenocrysts include euhedral crystals of zoned plagioclase (up to 62% An in the core) and amphibole ranging from Mg-hornblende to tschermakite (microprobe analytical data for rock-forming minerals can be presented upon request). The matrix is made up mainly of plagioclase microlites (An_{17-23}) and hornblende. Also present are irregularly scattered Fe-Ti oxides, minor flakes of biotite, interstitial grains of quartz (7–8 vol%), and alkali feldspar. The latter also occurs in rims around the plagioclase crystals. Microdiorite is variably altered to chlorite, micas, epidote, hematite, sericite, and clay minerals.

Lamprophyre (spessartite) is a dark-green pinkish fine- to medium-grained rock of lamprophyric texture. The only phenocrysts are tabular brownish green grains of Mg-hastingsite and Mg-hornblende. The amount of phenocrysts varies widely in different dikes, from 8 to 40 vol%. The fine-grained matrix of hypidiomorphic and prismatic granular texture consists mainly of plagioclase laths and subhedral brown amphibole grains, with secondary flakes of chloritized biotite. Alkali feldspar ($Or_{96}Ab_4$) forms rare interstitial grains and fine rims around plagioclase crystals; small quartz grains constitute ~2–3 vol% of the rock. Deuteric alteration is significant, and not infrequently epidote, chlorite, sericite, and carbonate are as abundant as magmatic minerals.

Suite 2. Although in appearance all rocks of this suite look fresh, the original minerals have been altered to a great extent both in the matrix and in phenocrysts. Significant sericitization and loss of Ca occurred in plagioclase; mafic minerals are replaced almost completely by aggregate of chlorite, epidote, opaque mineral, and calcite. Because of this, mineral composition of the rocks can be reconstructed roughly, and given characteristics are valid only for the least altered varieties.

Dacite porphyry is a fine-grained porphyritic rock of pinkish brown to dark pinkish gray color. It consists of feldspars (75–80 vol%), quartz (10–15%), mafic minerals, and Fe-Ti oxides (10–15% in total) and accessory apatite. The proportion of phenocrysts ranges from 15 to 30 vol% and more than 90% of them are feldspars. In less silicic varieties (60–63 wt% SiO_2), the main phenocryst is euhedral plagioclase surrounded in places by narrow alkali feldspar rims. As silica content increases, crystals of alkali feldspar constitute as much as 10–15% of the phenocrysts. The rest of the phenocrysts are Fe-Ti oxides and heavily altered mafic mineral (augite is rarely preserved). Fine-grained and very fine-grained matrix of hypidiomorphic and spherulitic texture is made up mainly of the same minerals as the phenocrysts, but always contains quartz. In the less silica-rich varieties, some wedge-shaped interstices are partly filled by green cryptocrystalline material similar to that in the andesite porphyry.

Andesite porphyry is a dark-gray porphyritic rock, with fine-grained matrix. Phenocrysts constitute from 10 to 25 vol% and include mainly 1 to 4-mm-long prisms of andesine (An_{41}) and rare smaller subhedral crystals of augite. In the matrix, along with dominant plagioclase, augite, and a significant amount of interstitial hypocrystalline material of chlorite composition (~15%), minor quartz and alkali feldspar (together about 5%), Fe-Ti oxide, and accessory apatite are present.

Fsp-rhyolite porphyry is a pinkish gray rock. Phenocrysts form from 2 to 7% of the rock volume and include euhedral crystals of alkali feldspar and albite. Phenocrysts of mafic minerals (biotite?) are extremely rare. The matrix texture is spherulitic, hypidiomorphic, in places microgranophyric.

Suite 3. *Quartz porphyry and Fsp-rhyolite porphyry* are grayish pink and brick red porphyritic rocks with fine-grained and aphyric matrix. They are mostly homogeneous, though clear fluidal texture is infrequently exhibited in dike margins. Miarolitic cavities and amigdules filled with quartz, calcite, and hydrobiotite constitute less than 1–2 vol%. The amount of phenocrysts, including quartz, alkali feldspar, and

rare albite, ranges from 2 to 15 vol%. In the Fsp-rhyolite porphyry, quartz phenocrysts are absent and albite phenocrysts are more common. The matrix is microgranophyric, cryptocrystalline, and spherulitic. It consists mainly of quartz and alkali feldspar, and evenly scattered needles of opaque mineral (up to 2–3 vol%). Mafic minerals (biotite and amphibole?) are completely replaced by hematite. Accessories are zircon and apatite. Alteration products include clay minerals, hematite, and carbonate.

Trachydolerite is a dark greenish gray, very fine-grained rock of microporphyritic texture. Phenocrysts amount from 3 to 5 vol%; their size is less than 0.5 mm. Elongated prisms of plagioclase (An_{51-55}) prevail. Also present are subhedral crystals of augite enriched in Mg and Ca. The matrix has typical dolerite texture defined by dominant plagioclase laths and rounded augite grains. Subordinate minerals are interstitial alkali feldspar with approximately equal amounts of Or and Ab components, and Fe-Ti oxide that is evenly distributed throughout the rock. Chlorite fills interstices between plagioclase laths. Apatite is a common accessory mineral.

Suite 4. *Trachydolerite* from suite 4 is very similar in appearance to dolerite from suite 3. However, alteration is so significant that reliable reconstruction of primary minerals is impossible. Only in one dike labradoritic plagioclase and augite are retained in phenocrysts; minerals of similar composition are found also in the matrix. Mostly magmatic minerals are completely transformed to albite, chlorite, epidote, and hematite.

GEOCHEMISTRY

The geochemical data set contains 111 analyses from the four successive dike suites. Of these, 24 samples were analyzed for rare earth elements (REE). Data for 60 representative samples are given in Tables 2 and 3. All samples are plotted in the classification and variation diagrams (Figs. 6–11). A full set of chemical data can be obtained from the authors by request via e-mail. A large part of the dike rocks, mostly from suites 2 and 4, is heavily altered to the extent that some mobile elements could be partially lost. Consequently the Nb/Y vs. $(Zr/TiO_2)*10^{-4}$ (Winchester and Floyd, 1977) based on less mobile elements is used for rock classification (Fig. 6).

Suite 1. Microdiorite corresponds to andesite and lamprophyre to andesite and andesite/basalt in Fig. 6. Since both contain alkali-feldspar they are referred to as trachyandesite and basaltic trachyandesite, respectively. In the K_2O vs. SiO_2 diagram (Fig. 7), compositions of both rock types straddle the medium-K and high-K fields of the calc-alkaline series. In many microdiorite samples the value of Na_2O-2 is $\geq K_2O$; this points to their sodic character, according to the IUGS classification (Le Maitre, 1989). Microdiorite is high-Al ($Al_2O_3 > 16$ wt%) and its #Mg value is commonly <50, whereas in lamprophyre the Al_2O_3 content ranges from 14.4 to 16.2 wt% and the #Mg value is >60 (Table 2). Compared with microdiorite, lamprophyre is enriched in MgO and FeO^T, and contains less SiO_2, Sr, and Zr (Fig. 7). REE patterns (Fig. 8a) in rocks of this suite display mild LREE enrichment and relatively flat HREE pattern; La/Yb_N ratio is ~11 in microdiorite and ~7 in lamprophyre. Negative Eu anomalies are actually absent (Table 3).

Suite 2. Rock types of this suite form an almost continuous compositional sequence from andesite porphyry through dacite porphyry to Fsp-rhyolite porphyry (Fig. 6). The K_2O content is typical of calc-alkaline high-K rocks (Fig. 7). In the mafic varieties, $Na_2O-2< K_2O$ (Table 2), which is characteristic of latite in the IUGS classification. In the Fsp-rhyolite porphyry K_2O dominates over Na_2O (Table 2).

The variation diagrams relative to SiO_2 (Fig. 7) demonstrate negative correlation trends for CaO, Sr, Al_2O_3, MgO, FeO*, as well as for TiO_2 (not shown) whereas trends for Zr, and less clearly for K_2O and Rb are positive. Also positive and similar to Zr are trends for Nb and Y (not shown). REE patterns for mafic and silicic rocks are sub-parallel and show a clear tendency to increase of ΣREE with SiO_2 increase (Tables 2 and 3; Fig. 8b). The La/Yb_N ratio is about 3–10; the Eu/Eu* value ranges from 0.82 in mafic to 0.37 in silicic rocks; it is positively correlated with Sr and Ca (Fig. 8b). The demonstrated correlations of major and trace elements (Figs. 7,8) suggest that the evolution of the dike rock compositions was controlled mainly by fractionation of plagioclase, which is the dominant phenocryst both in andesite porphyry and dacite porphyry, and of small amounts of pyroxene and Fe-Ti oxides.

Chemical compositions of dike-like rocks collected from boulder-size clastic fragments in the Elat conglomerate that overlies the dike suite 2 are given in Tables 2–3 and Fig. 7. Both mafic and felsic rocks from pebbles are chemically similar to corresponding rock types making up dikes of suite 2. This is true for most major and trace elements (Fig. 7).

Suite 3. The dominant *silicic dikes* include quartz porphyry and subordinate Fsp-rhyolite porphyry.

Table 2

Chemical composition of representative dike rocks, major (wt%) and selected trace elements (ppm)

Rock	MD-1	MD-1	MD-1	MD-1	MD-1	MD-1	Lmp-1	Lmp-1	Lmp-1	Lmp-1	Lmp-1	And-2	And-2	And-2	And-2
sample no.	62-6	31*	27	163	35-4*	173-a	25	165-2	20	10-1	20-4*	148*	150	36*	228-1
SiO_2	57.50	58.25	58.5	58.80	59.30	60.00	52.10	52.2	53.3	53.6	54.30	54.70	54.8	55.50	55.80
TiO_2	0.98	0.92	1.04	1.05	0.89	0.92	1.10	1.01	0.86	0.84	0.85	1.13	1.09	1.08	1.21
Al_2O_3	19.15	18.50	16.9	18.00	17.40	16.2	16.20	14.45	15.6	16.2	16.00	16.90	17.5	17.20	16.00
Fe_2O_3	2.49	2.66	3.38	3.52	2.23	2.94	2.90	3.05	2.11	2.37	2.23	7.60	3.32	2.81	6.89
FeO	3.11	3.11	3.43	2.94	3.43	3.01	5.74	4.58	5.84	5.58	5.66	0.13	3.35	3.67	0.73
MnO	0.09	0.08	0.09	0.09	0.11	0.1	0.13	0.12	0.12	0.12	0.13	0.10	0.1	0.12	0.10
MgO	2.62	2.56	2.66	2.69	3.07	3.59	7.06	9.69	7.65	7.94	6.59	4.75	4.93	4.80	3.89
CaO	5.45	4.22	5.34	3.73	3.94	3.99	4.78	5.09	5.23	5.59	5.69	4.00	3.74	2.69	2.26
Na_2O	4.38	4.60	4.16	4.74	4.56	4.36	4.38	3.35	4.06	3.57	3.52	3.93	3.83	4.43	5.76
K_2O	2.08	2.16	1.93	2.62	2.62	2.65	1.75	1.28	2.02	1.66	2.07	2.45	2.66	3.06	2.77
P_2O_5	0.29	0.30	0.28	0.33	0.26	0.26	0.28	0.34	0.22	0.21	0.24	0.32	0.31	0.30	0.30
LOI	2.14	2.44	1.58	1.62	2.08	2.1	3.74	4.6	2.74	2.61	2.72	3.54	4.49	4.40	3.84
Total	100.28	99.80	99.29	100.13	99.89	100.12	100.16	99.76	99.75	100.29	100.00	99.55	100.12	100.06	99.55
Rb	50	60	49	76	70	78	56	29	60	51	66	90	96	110	55
Ba	750	840	670	960	1000	770	490	670	580	570	690	570	470	580	930
Sr	730	700	690	650	630	580	360	550	410	540	520	460	450	390	200
Zr	170	190	180	200	170	170	130	200	120	120	140	200	200	170	200
Nb	10	8	8	11	6	8	9	8	4	4	5	11	11	10	8
Y	24	18	22	20	16	20	26	17	19	17	21	26	22	22	25
#Mg	46.6	45.3	42.3	44.0	50.2	53.1	60.1	70.2	63.8	64.8	60.5	54.9	58.1	58.0	50.0
$(Na_2O-2)-K_2O$	0.3	0.4	0.23	0.1	–0.1	–0.29	0.6	0.07	0.0	–0.09	–0.6	–0.5	–0.83	–0.6	1.0

Abbreviations (numbers denote the dike suite): MD = microdiorite; Lmp = lamprophyre; And = andesite porphyry; Dac = dacite porphyry; RhP = rhyolite porphyry; QtzP = quartz porphyry; D-mTi and D-hTi = trachydolerite moderate and high-Ti, respectively; FCong = clastic fragment in Elat conglomerate.

#Mg = 100 MgO/(MgO+FeO*), mol% and $(Na_2O-2)-K_2O$, wt% were calculated in mafic rocks.

REE and selected trace element contents for samples marked with asterisk are given in Table 3.

Table 2 *continued*

Rock	Dac-2	Dac-2	Dac-2	Dac-2	Dac-2	Dac-2	Dac-2	Dac-2	Dac-2	RhP-2	RhP-2	RhP-2	RhP-2	RhP-2
sample no.	227-1	170	168	244	153*	147*	159	154*	163-1	201	198-2	D-42*	227	148-1
SiO_2	57.8	58.2	60.0	61.9	62.00	62.40	62.30	67.9	68.5	73.7	71.1	71.1	76.5	77.1
TiO_2	0.95	1.06	1.02	1.02	0.88	0.98	0.89	0.60	0.55	0.17	0.34	0.3	0.12	0.1
Al_2O_3	15.6	17.9	16.45	15.2	15.65	14.70	15.80	14.85	15	13.85	12.85	13.7	11.3	11.3
Fe_2O_3	5.87	2.72	5.06	5.93	4.52	5.01	5.06	3.63	3.23	0.69	2.6	3.3[1]	1.9	1.77
FeO	0.5	2.68	0.78	0.11	1.19	0.82	0.15	0.15	0.07	0.79	0.45	n.d.	–	0.08
MnO	0.1	0.1	0.18	0.13	0.08	0.08	0.08	0.12	0.05	0.05	0.04	0.04	0.07	0.02
MgO	3.73	2.94	2.1	1.82	2.08	1.46	2.07	0.80	0.66	0.31	0.44	0.4	0.14	0.1
CaO	2.22	2	2.05	2	1.89	2.56	2.25	0.65	1.1	0.38	0.93	0.8	0.29	0.2
Na2O	5.29	5.55	5.53	5.45	5.34	5.11	5.49	5.21	5.24	4.51	3.78	4.1	3.33	3.61
K_2O	3.56	3.47	3.56	3.64	3.47	3.58	3.20	4.30	4.21	4.72	5.69	4.7	5.33	4.89
P_2O_5	0.24	0.29	0.35	0.3	0.03	0.31	0.25	0.17	0.12	0.05	0.06	0.05	0.03	0.03
LOI	3.61	2.83	2.78	2.46	2.45	2.58	2.40	1.12	1.3	0.74	1.57	–	0.42	0.22
Total	99.47	99.74	99.86	99.96	99.58	99.59	99.94	99.50	100.03	99.96	99.85	98.49	99.4	99.39
Rb	115	97	97	100	97	90	80	98	110	110	140	130	185	175
Ba	650	820	940	860	920	800	750	920	1000	960	550	770	90	90
Sr	260	420	280	210	270	220	210	130	140	180	87	100	30	57
Zr	280	290	270	290	310	280	300	350	430	160	490	–	630	580
Nb	11	14	17	12	15	16	13	17	19	8	31	14	36	31
Y	22	27	24	31	28	35	28	33	34	23	40	40	76	70
#Mg														
$(Na_2O\text{-}2)\text{-}K_2O$														

Abbreviations (numbers denote the dike suite): MD = microdiorite; Lmp = lamprophyre; And = andesite porphyry; Dac = dacite porphyry; RhP = rhyolite porphyry; QtzP = quartz porphyry; D-mTi and D-hTi = trachydolerite moderate and high-Ti, respectively; FCong = clastic fragment in Elat conglomerate.
#Mg = 100 MgO/(MgO+FeO*), mol% and $(Na_2O\text{-}2)\text{-}K_2O$, wt% were calculated in mafic rocks.
REE and selected trace element contents for samples marked with asterisk are given in Table 3.

Table 2 *continued*

Rock	FCong	FCong	FCong	FCong	FCong	FCong	QtzP-3	QtzP-3	QtzP-3	QtzP-3	QtzP-3	QtzP-3	QtzP-3	QtzP-3	RhP-3
sample no.	131*	131-6	131-3*	131-4	131-1	249	18*	155	66-3*	150-1*	157	128*	144-2*	239	35-6
SiO_2	56.00	58.80	70.8	71.70	75.00	77.30	74.70	76.10	76.20	76.40	76.70	77.00	77.20	78.40	72.10
TiO_2	1.30	0.95	0.3	0.16	0.09	0.06	0.14	0.14	0.13	0.13	0.15	0.10	0.10	0.10	0.20
Al_2O_3	16.90	17.60	14.2	13.90	12.80	11.50	11.20	11.60	11.60	11.10	11.30	11.90	11.70	10.10	13.30
Fe_2O_3	3.05	4.42	2.33	2.87	1.52	1.21	2.60	2.20	2.74	1.85	2.85	1.65	1.97	1.98	2.73
FeO	5.29	2.19	0.45	0.19	0.13	0.26	0.16	0.00	0.18	0.19	0.07	0.15	0.11	0.11	0.08
MnO	0.13	0.09	0.05	0.04	0.03	0.03	<0.01	0.02	0.01	0.01	0.02	0.01	0.06	0.02	0.04
MgO	4.44	2.52	0.38	0.35	0.24	0.25	0.10	0.20	0.13	0.23	0.17	0.29	0.06	0.05	0.29
CaO	2.89	2.00	1.26	0.78	0.41	0.36	1.13	0.20	0.19	0.55	0.01	0.48	0.14	0.48	1.00
Na_2O	3.60	5.86	4.19	4.06	3.30	2.96	3.72	3.89	3.00	3.46	2.72	3.90	3.41	2.58	5.41
K_2O	3.58	2.88	5.06	5.00	5.57	5.69	3.88	4.17	5.40	5.00	5.48	4.08	4.92	5.35	3.80
P_2O_5	0.33	0.25	0.33	0.04	0.03	<0.05	0.02	0.04	<0.01	0.05	0.03	0.01	0.01	0.02	0.02
LOI	2.06	2.64	1.05	0.88	0.41	0.39	2.12	1.00	0.82	0.82	0.74	0.56	0.39	0.43	1.08
Total	99.57	100.20	100.4	100	100	100	99.77	100	100.40	99.79	100	100.13	100	100	100.03
Rb	81	77	140	125	160	170	135	105	194	170	190	140	150	180	88
Ba	670	780	1080	980	810	660	50	210	150	180	180	70	190	200	800
Sr	320	270	150	130	110	90	50	35	60	43	55	13	27	38	28
Zr	200	170	400	400	125	105	590	490	590	630	570	600	590	560	380
Nb	11	8	19	17	14	10	35	23	34	35	34	29	33	31	18
Y	32	23	42	40	17	13	68	77	75	75	68	78	68	64	42
#Mg	46.6														
$(Na_2O\text{-}2)\text{-}K_2O$	−1.98														

Abbreviations (numbers denote the dike suite): MD = microdiorite; Lmp = lamprophyre; And = andesite porphyry; Dac = dacite porphyry; RhP = rhyolite porphyry; QtzP = quartz porphyry; D-mTi and D-hTi = trachydolerite moderate and high-Ti, respectively; FCong = clastic fragment in Elat conglomerate.

#Mg = 100 MgO/(MgO+FeO*), mol% and $(Na_2O\text{-}2)\text{-}K_2O$, wt% were calculated in mafic rocks.

REE and selected trace element contents for samples marked with asterisk are given in Table 3.

Table 2 *continued*

Rock sample no.	RhP-3 147-2*	RhP-3 156-1*	RhP-3 245	RhP-3 D-40	D mTi-3 196-1*	D mTi-3 N-1*	D hTi-3 198-1	D hTi-3 D-21aa*	D hTi-4 166*	D hTi-4 AM-3	D hTi-4 AM-15*	D hTi-4 MR-6*	D hTi-4 MR-203
SiO_2	73.30	70.20	77.6	76.3	50.80	52.80	49.30	50.47	45.80	49.00	46.60	47.50	47.30
TiO_2	0.20	0.39	0.09	0.14	1.83	1.72	2.88	2.77	3.34	4.09	4.51	4.18	4.26
Al_2O_3	12.95	14.55	11.1	11.5	15.30	14.70	14.70	14.75	13.15	14.00	13.80	14.20	14.40
Fe_2O_3	2.47	2.74	2.17	2.58	3.44	4.82	6.57	11.56	11.60	12.1'	13.3'	14.9'	13.9'
FeO	0.15	0.11	0.08	0.07	4.35	4.10	4.35	0.00	1.82	n.d	n.d	n.d	n.d
MnO	0.06	0.04	0.01	0.03	0.17	0.18	0.14	0.10	0.10	n.d	n.d	0.19	0.16
MgO	0.30	0.61	0.1	0.25	4.47	4.60	4.99	4.37	4.28	8.36	5.08	4.26	4.35
CaO	0.38	0.44	0.3	0.44	6.28	6.00	4.30	3.20	6.44	2.39	8.14	7.22	7.55
Na_2O	5.11	5.19	4.5	4.00	3.79	3.27	3.83	3.32	3.68	2.54	3.07	3.29	3.28
K_2O	4.00	4.08	3.38	3.83	3.78	2.76	3.22	3.36	2.42	2.90	1.45	1.59	1.76
P_2O_5	0.05	0.10	<0.05	0.04	0.38	0.40	1.07	1.19	1.80	0.87	1.00	0.94	1.03
LOI	0.50	1.08	0.27	0.64	5.44	4.65	5.02	5.05	5.32	3.59	3.26	1.33	1.91
Total	99.47	99.53	99.6	99.82	100.03	100.00	100.37	100.14	99.75	99.84	100.21	99.63	99.90
Rb	84	96	88	89	86	65	73	102	61	54	30	29	33
Ba	760	840	140	760	940	750	840	657	1000	559	536	607	613
Sr	25	96	17	58	460	430	400	167	540	230	583	520	525
Zr	390	360	440	350	210	220	280	318	260	345	297	321	335
Nb	18	16	21	17	13	18	14	22	23	42	35	39	41
Y	37	31	50	35	28	26	45	48	50	39	44	44	44
#Mg	–	–	–	–	51.7	49.3	46.4	42.8	38.4	57.8	43.1	36.2	38.3
(Na2O-2)-K2O	–	–	–	–	–2.0	–1.5	–1.4	–2.0	–0.7	–2.4	–0.4	–0.3	–0.5

Abbreviations (numbers denote the dike suite): MD = microdiorite; Lmp = lamprophyre; And = andesite porphyry; Dac = dacite porphyry; RhP = rhyolite porphyry; QtzP = quartz porphyry; D-mTi and D-hTi = trachydolerite moderate and high-Ti, respectively; FCong = clastic fragment in Elat conglomerate.

#Mg = 100 MgO/(MgO+FeO*), mol% and $(Na_2O-2)-K_2O$, wt% were calculated in mafic rocks.

Agpaitic index: NK/A = $(Na_2O+K_2O)/Al_2O_3$, mol%.

Samples AM-3 and AM-15 from Kessel (1995); samples MR-6 and MR-203 from Mushkin et al. (2003).

REE and selected trace element contents for samples marked with asterisk are given in Table 3.

Table 3
REE and selected trace element contents in representative dike rocks (ppm)

Sample	MD-1	MD-1	Lmp-1	And-2	And-2	Dac-2	Dac-2	Dac-2	RhP-2	FCong	FCong	QtzP-3	QtzP-3	QtzP-3
no.	31	35-4	20-4	148	36	153	147	154	D-42	131	131-3	18	66-3	150-1
La	24.0	22.8	13.5	19.3	17.5	29.2	31.1	19.9	20.0	22.2	40.5	60.0	43.4	27.0
Ce	54.8	52.5	30.5	43.2	39.7	58.8	64.1	64.5	90.0	52.3	84.4	120.0	102.2	78.7
Pr	6.7	6.5	3.8	5.3	4.9	7.1	8.1	5.6	6.1	6.2	10.3	14.0	12.2	8.6
Nd	26.8	25.1	15.9	21.2	20.1	27.4	31.4	22.6	25.0	25.7	40.3	55.0	49.8	35.1
Sm	5.1	4.9	3.3	4.3	4.1	5.4	6.1	5.1	6.0	5.4	7.8	11.5	11.6	8.7
Eu	1.47	1.41	0.97	1.08	1.07	1.23	1.20	1.06	0.70	1.30	1.29	0.30	0.28	0.20
Gd	4.30	4.05	2.91	3.80	3.67	4.58	5.31	4.81	5.60	4.79	6.54	11.0	11.00	9.05
Tb	0.60	0.59	0.43	0.56	0.55	0.67	0.78	0.77	1.00	0.72	1.02	1.90	1.93	1.55
Dy	3.08	3.13	2.54	3.24	3.21	3.90	4.68	4.72	6.50	4.21	6.26	11.00	11.19	10.22
Ho	0.58	0.59	0.55	0.71	0.68	0.85	1.02	1.04	1.30	0.92	1.39	2.30	2.33	2.23
Er	1.63	1.63	1.46	1.88	1.79	2.23	2.67	2.88	4.20	2.41	3.79	6.90	6.73	6.07
Tm	0.22	0.23	0.22	0.27	0.26	0.33	0.41	0.43	0.70	0.35	0.57	0.98	1.02	0.91
Yb	1.53	1.54	1.41	1.66	1.63	2.09	2.57	2.79	4.40	2.25	3.66	6.50	6.57	5.72
Lu	0.22	0.23	0.21	0.25	0.24	0.33	0.38	0.42	0.57	0.34	0.57	0.98	0.98	0.84
ΣREE	131	125	78	107	99	144	160	137	172	129	208	302	261	195
Eu/Eu*	0.96	0.97	0.96	0.82	0.84	0.76	0.64	0.66	0.37	0.78	0.55	0.08	0.08	0.07
(La/Yb)N	11	11	7	8	8	10	9	5	3	7	7	7	5	3
Hf	4.3	4.1	2.7	3.7	3.7	5.8	5.7	7.1	n.d.	4.3	9.6	14.0	14.4	13.2
Ta	0.8	2.0	0.9	0.7	0.7	1.2	7.5	1.9	4.4	0.8	3.3	3.0	2.8	3.7
Th	3.9	4.7	2.2	4.6	4.5	7.2	8.0	9.0	n.d.	5.4	11.4	17.3	17.7	15.2
U	1.1	1.4	0.7	1.3	1.3	2.5	2.6	3.9	n.d.	1.7	3.7	4.7	5.7	5.0
Ga	24	26	14	16	15	15	17	19	n.d.	18	12	21	19	16
V	112	150	122	116	128	50	45	11	n.d.	182	17	45	54	20
Cu	29	16	23	24	22	6	34	7	n.d.	20	36	7	10	5
Pb	12	15	6	25	11	21	35	27	n.d.	9	5	13	65	27
Zn	82	89	61	101	156	103	131	74	n.d.	114	31	37	37	59
Sc	8	11	17	15	15	10	11	8	n.d.	20	9	n.d.	n.d.	1
Cs	2	8	2	7	5	2	1	2	n.d.	4	2	1	1	2

Table 3 *continued*

Sample no.	QtzP-3 128	QtzP-3 144-2	RhP-3 147-2	RhP-3 156-1	D mTi-3 196-1	D mTi-3 N-1	D hTi-3 D-21aa	D hTi-4 166	D hTi-4 AM15	D hTi-4 MR-6
La	29.3	39.3	31.8	17.5	24.0	28.4	34.1	38.1	47.5	40.0
Ce	69.4	89.2	87.7	66.2	52.0	57.9	81.9	90.6	117.0	91.0
Pr	8.7	10.5	8.4	4.7	7.1	6.8	11.0	12.2	13.1	12.0
Nd	34.9	41.0	32.0	19.5	30.0	27.7	50.0	55.3	60.8	52.0
Sm	8.8	9.8	6.2	5.0	6.1	5.6	11.0	12.0	12.8	11.0
Eu	0.14	0.18	0.82	0.87	1.50	1.58	3.19	5.94	3.72	3.50
Gd	8.76	9.40	5.24	4.88	6.36	5.23	10.13	11.46	10.70	11.00
Tb	1.53	1.63	0.83	0.84	0.80	0.81	1.53	1.60	1.44	1.50
Dy	39.76	10.30	5.21	5.12	4.23	4.69	7.94	8.96	7.71	7.50
Ho	2.18	2.31	1.17	1.13	0.80	0.94	1.50	1.82	1.43	1.40
Er	6.01	6.32	3.18	3.01	2.35	2.60	3.95	4.34	3.62	3.80
Tm	0.90	0.95	0.49	0.46	0.33	0.37	0.53	0.58	0.51	0.50
Yb	5.65	5.92	3.08	3.03	1.96	2.45	3.37	3.36	3.14	2.90
Lu	0.83	0.90	0.49	0.47	0.29	0.37	0.48	0.48	0.45	0.40
ΣREE	187	228	187	133	138	145	221	247	284	239
Eu/Eu*	0.05	0.06	0.44	0.54	0.74	0.89	0.92	1.55	0.97	0.97
$(La/Yb)_N$	4	5	7	4	9	8	7	8	11	10
Hf	13.2	13.7	7.7	7.8	5.2	4.7	6.8	5.6	n.d	n.d
Ta	3.6	7.4	1.9	2.2	1.2	0.6	1.5	1.6	n.d	3.0
Th	15.4	17.0	9.4	10.5	4.2	3.7	4.5	3.3	4.3	4.3
U	4.1	5.6	3.5	3.5	1.2	0.8	1.5	2.0	0.9	1.3
Ga	20	21	17	17	23	20	34	22	31	24
V	2	5	5	5	206	165	161	184	198	276
Cu	3	6	5	5	47	43	7	31	180	118
Pb	8	26	19	18	11	10	11	17	n.d	14
Zn	55	35	56	66	97	104	348	140	337	175
Sc	1	1	8	7	n.d.	n.d.	n.d.	26	n.d	n.d
Cs	1	2	4	1	2	2	1	1	n.d.	n.d.

Abbreviations as in Table 2.

Sample AM-15 after Kessel, 1995; sample MR-6 from Mushkin et al., 2003.

Eu* = (Sm*Gd)½. n.d. = concentration of element was not determined.

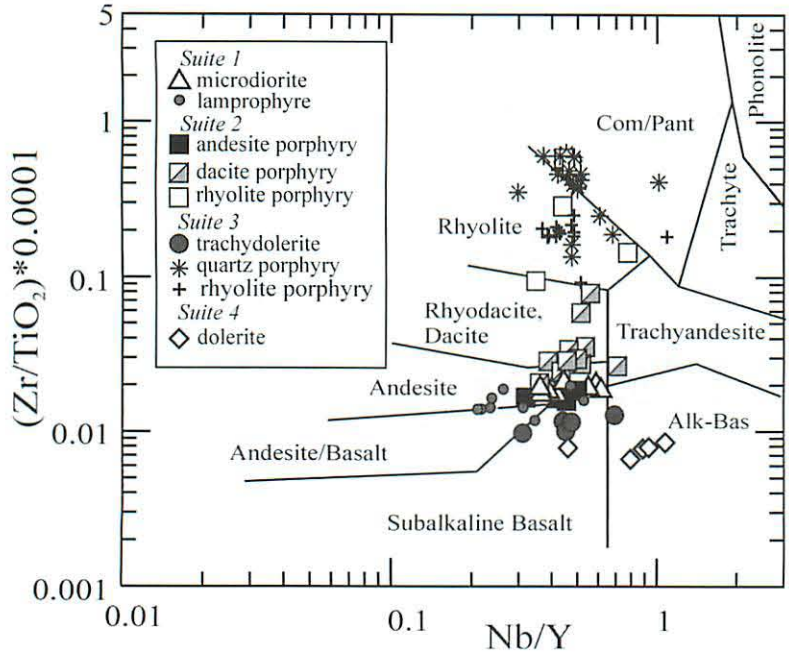

Fig. 6. Dike rock compositions plotted on the Nb/Y vs. [(Zr/TiO_2)*0.0001] classification diagram, after Winchester and Floyd (1977).

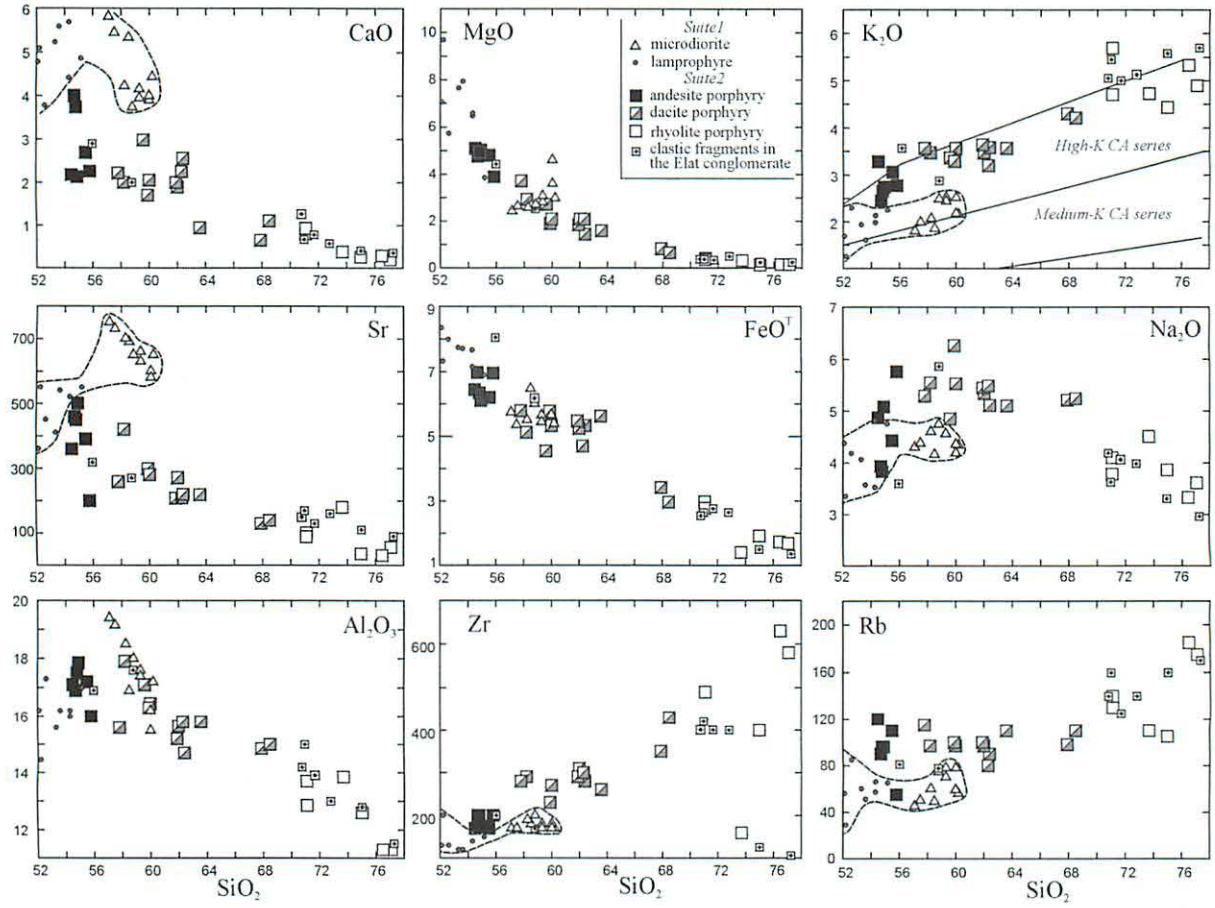

Fig. 7. Silica variation diagrams for dike rocks from suites 1 and 2. In the K_2O vs. SiO_2 diagram the boundary lines are after Le Maitre (1989) and Rickwood (1989).

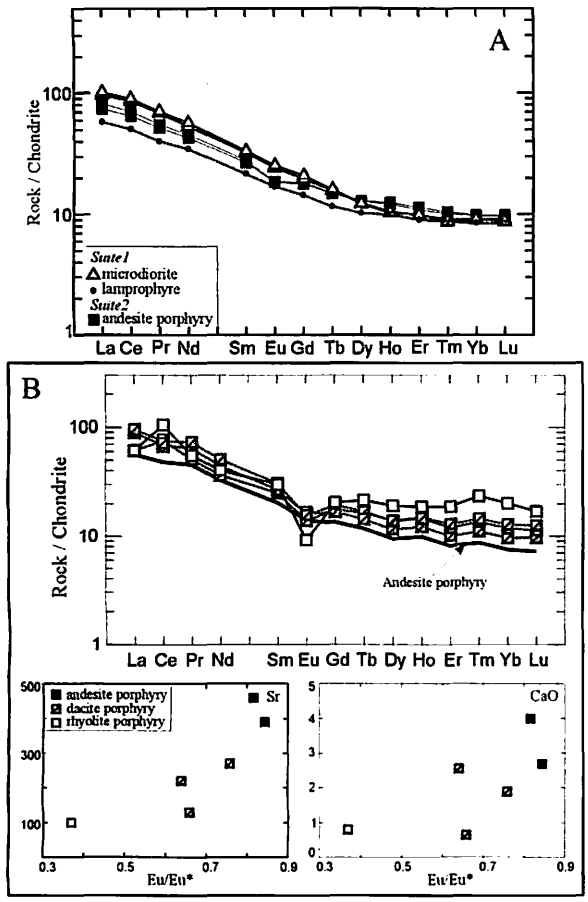

Fig. 8. A = Chondrite-normalized REE patterns for mafic rocks from dike suites 1 and 2; B = REE patterns, Eu/Eu* vs. Sr and CaO diagrams for andesite (average), dacite, and rhyolite porphyry from dike suite 2. Here and in the other figures, chondrite values are after Sun and McDonough (1989).

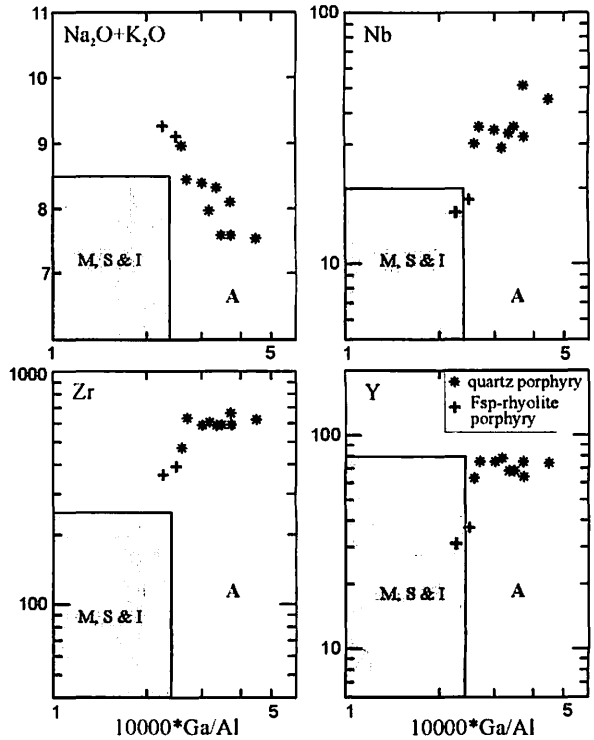

Fig. 9. Ga/Al vs. $Na_2O + K_2O$, Nb, Zr, and Y diagrams for silicic rocks from dike suite 3. Rectangles denote the fields of S-, I-, and M-type granitoids; A = A-type granite (after Whalen et al., 1987).

Silicic rocks are alkaline (the agpaitic index *NK/A* is >0.9) and are referred to as typical A-type granite (Fig. 9).

In silica variation diagrams both quartz porphyry and Fsp-rhyolite porphyry do not show clear trends, so that their mutual arrangement in the plots cannot be regarded as evidence of magma differentiation (Fig. 10). Quartz porphyries form slightly elongated clusters in variation diagrams and a distinct field in the REE abundance patterns (Fig. 10). They are characterized by higher contents of K_2O, Rb, Zr, Y, and REE, and lower contents of Na_2O and Ba relative to Fsp-rhyolite porphyry. An unusual chemical feature of Fsp-rhyolite porphyry is enhanced Ba, even though K_2O and Rb are lower and Na_2O is higher than in quartz porphyry (Fig. 10). Quartz porphyry is richer in REE, and negative Eu anomaly for this rock type is much more pronounced: Eu/Eu* values are 0.05–0.08 vs. 0.44–0.54 (Fig. 11, Table 3). This shows that the quartz porphyry magma was highly differentiated. Lower concentration of REE in the Fsp-rhyolite may reflect lower abundance of accessory minerals, which is manifested in lower Zr and Y (Fig. 10). Although the Fsp-rhyolite from suite 3 is very similar to Fsp-rhyolite from suite 2 in mineral composition and texture, this rock type can be readily distinguished by K_2O, Na_2O, and Rb contents, as shown in Fig. 10.

Mafic members of the suite are trachydolerite and rare trachyandesite porphyry. Andesitic rocks frequently exhibit evidence of hybrid origin (magma mixing); their chemistry will be discussed elsewhere. On a K_2O–SiO_2 plot the trachydolerite compositions are confined to the fields of high-K calc-alkaline and shoshonitic series. Two subgroups of trachydolerites are distinguished by TiO_2 content, high-Ti and moderate-Ti with 2.8–2.9 and 1.7–1.8 wt% TiO_2, respectively (Table 2). Rocks of both subgroups are mostly low-Al (Al_2O_3 = 14.7–15.6 wt%), with comparatively low MgO, from 4.3 to 5 wt%. They are similar in SiO_2 content (49.3–52.8 wt%), as well as in Ba and Na_2O,

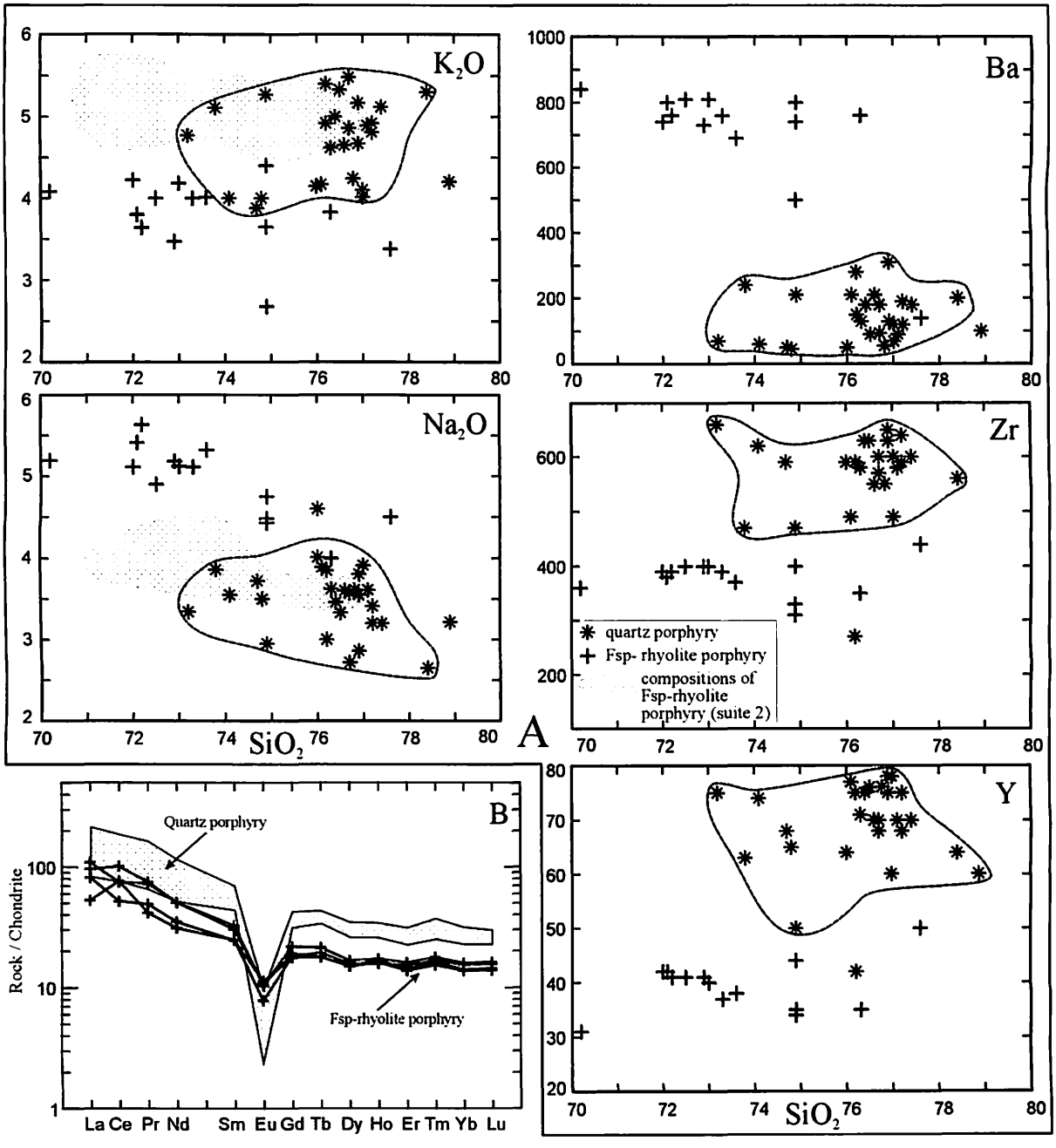

Fig. 10. Silica variation diagrams (A) and REE patterns (B) for silicic rocks from dike suite 3.

whereas high-Ti trachydolerite is noticeably richer in P_2O_5, Zr, Y, and FeO^T and contains less Sr (Fig. 11A; Table 2). The REE patterns of both subgroups are gently dipping and almost parallel (Fig. 11B). High-Ti dolerite is richer in ΣREE.

Suite 4. In the central Elat area rocks of this suite are mostly heavily altered, so we used both our own data and published chemical analyses of trachydolerites from the adjacent Amram block (Kessel, 1995; Kessel et al., 1998; Mushkin et al., 2003). The chemical characterization of the trachydolerites from suite 4 should thus be regarded as preliminary. They differ from trachydolerites of suite 3 by higher Ti (3.3–4.5 wt%), FeO*, Zr, and Nb contents; REE patterns overlap almost entirely (Fig. 11). Commonly Eu anomalies are inconspicuous, however, a positive

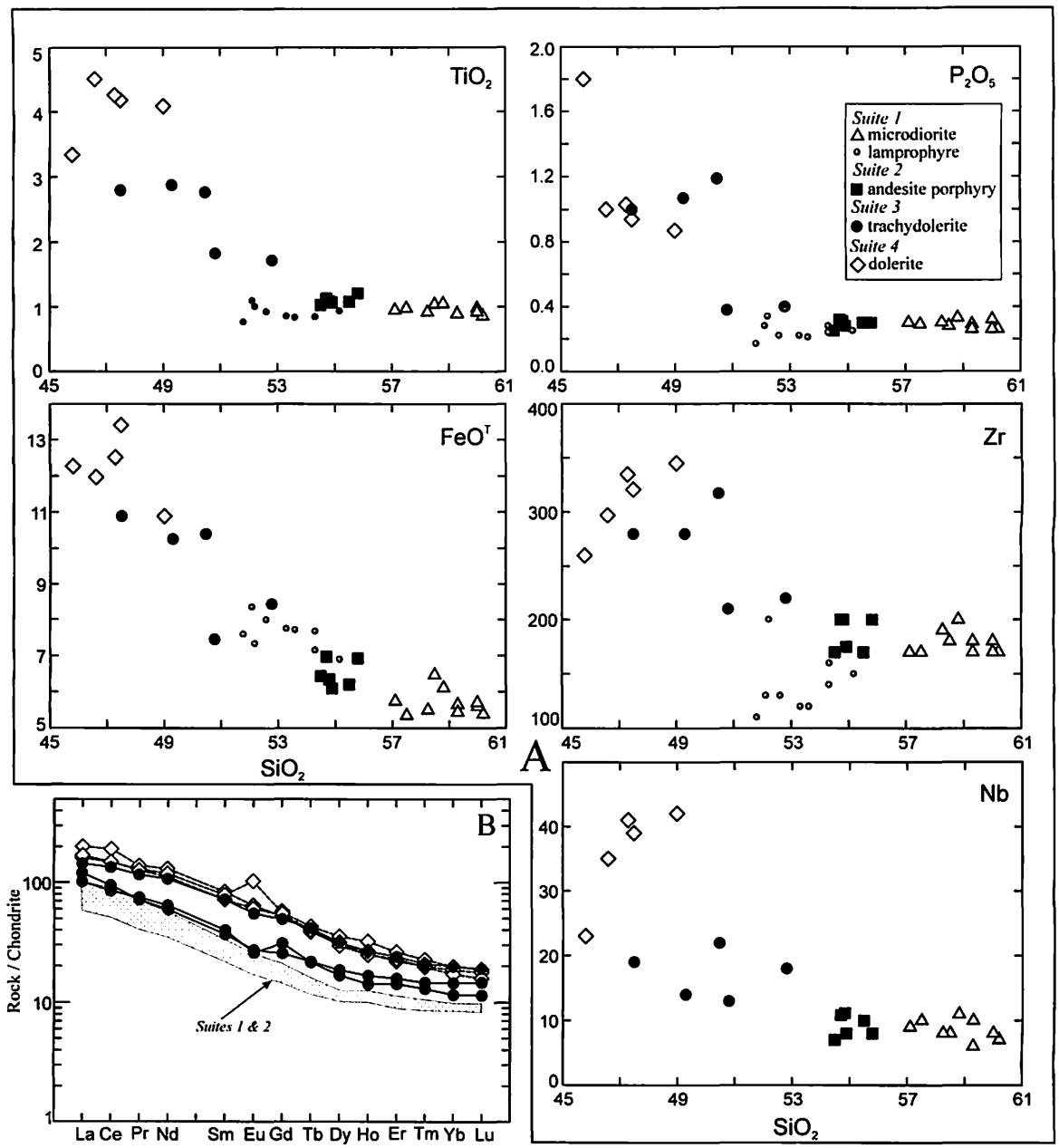

Fig. 11. Silica variation diagrams (A) and REE patterns (B) illustrating the chemical discrimination between calc-alkaline (suites 1 and 2) and mildly alkaline (suites 3 and 4) mafic dikes.

Eu anomaly suggesting the presence of cumulate plagioclase crystals is revealed in one dolerite sample (Fig. 11, Table 3).

DISCUSSION

The sequence of dike suites established in the central Elat area is more or less comparable with the dike sequence proposed by Stein, Navon, and Kessel (Kessel, 1995; Stein et al., 1997; Kessel et al., 1998). However, the distinction is significant. We found that the calc-alkaline dike suite recognized by Stein and coworkers includes two successive calc-alkaline suites. The first one consists of amphibole-bearing microdiorite and lamprophyre, and the second suite incorporates mainly dacite porphyry with subordinate rhyolite porphyry and Cpx-bearing trachyandesite porphyry. We also found that the basic rocks of suites TH1 and

Table 4
Average chemical composition of the mafic rocks from four successive dike suites (Elat area) and from southern Sinai (wt% and ppm)

Rock	MD-1 (10, 2)*	Lmp-1 (9, 1)	And-2 (6, 2)	D mTi-3 (3, 2)	D hTi-3 (3, 1)	D mTi-4 3	D hTi-4 (3, 3)	AmphD (16, 16)	CpxD (47, 47)	D (5, 5)
SiO_2	58.90	53.52	55.03	51.07	49.09	48.27	47.24	57.16	48.41	47.74
TiO_2	0.95	0.90	1.10	1.90	2.82	2.13	4.08	1.4	3.06	2.78
Al_2O_3	17.59	15.80	17.09	15.20	14.68	15.33	13.91	16.29	13.67	14.74
Fe_2O_3	2.71	2.28	4.99	4.05	10.08	8.61	13.16	–	–	5.34
FeO	3.26	5.43	2.01	4.79	4.35	1.67	1.82	7.56	14.62	7.64
MnO	0.10	0.12	0.11	0.19	0.11	0.04	0.15	0.13	0.2	0.20
MgO	3.00	7.32	4.75	5.16	4.55	5.54	5.27	4.95	7.04	4.82
CaO	4.50	5.10	2.83	6.45	4.50	5.86	6.35	7.19	7.67	6.95
Na_2O	4.42	3.87	4.65	3.60	3.68	3.71	3.17	3.43	2.58	3.56
K_2O	2.31	1.93	2.83	2.76	3.19	2.18	2.02	1.78	1.43	1.71
P_2O_5	0.29	0.24	0.29	0.40	1.09	0.78	1.13	0.38	1.32	1.03
LOI	1.93	3.27	4.13	4.54	5.04	4.70	3.08	–	–	3.14
Total	99.93	99.77	99.81	100.11	98.60	98.83	99.87	100	100	99.65
Rb	62	56	95	63	85	58	41	53	37	49
Ba	875	612	623	750	729	924	663	504	838	872
Sr	664	474	393	483	232	503	480	683	560	644
Zr	178	140	186	210	293	273	325	143	288	291
Nb	9	6	9	14	18	19	36	9	26	22
Y	19	20	23	26	45	30	44	27	59	49
Hf	4.2	2.7	3.7	4.9	6.8	–	5.6	–	–	7.5
Ta	1.4	0.9	0.7	0.9	1.5	–	2.3	–	–	1.4
Th	4.3	2.2	4.5	4.0	4.5	–	4.1	–	–	–
La	23.4	13.5	18.4	26.2	34.1	–	41.9	22	41	40.2
Ce	53.6	30.5	41.5	54.9	81.9	–	99.5	56	102	98.2
Pr	6.6	3.8	5.1	7	11	–	12.5	–	–	11.4
Nd	25.9	15.9	20.6	28.8	50	–	56.0	29	60	54.8
Sm	5.0	3.3	4.2	5.9	11	–	11.9	–	–	13.6
Eu	1.44	0.97	1.07	1.54	3.19	–	4.39	–	–	3.81
Gd	4.18	2.91	3.73	5.80	10.13	–	11.05	–	–	10.64
Tb	0.60	0.43	0.55	0.81	1.53	–	1.51	–	–	1.16
Dy	3.11	2.54	3.22	4.46	7.94	–	8.06	–	–	9.56
Ho	0.59	0.55	0.69	0.87	1.50	–	1.55	–	–	1.70
Er	1.63	1.46	1.84	2.48	3.95	–	3.92	–	–	4.86
Tm	0.23	0.22	0.26	0.35	0.53	–	0.53	–	–	–
Yb	1.54	1.41	1.65	2.21	3.37	–	3.13	–	–	4.02
Lu	0.23	0.21	0.24	0.33	0.48	–	0.44	–	–	0.56
$(Na_2O-2)-K_2O$	0.1	–0.1	–0.2	–1.2	–1.5	–0.5	–0.9	–	–	–0.2
ΣREE	128	78	103	141	219	–	256	–	–	255
$(La/Yb)_N$	11	7	8	9	7	–	10	–	–	7

Abbreviations. *Elat area* (numbers denote the dike suite): MD = microdiorite, Lmp = lamprophyre, And = andesite porphyry, D-mTi and D-hTi = trachydolerite moderate and high-Ti, respectively. *Southern Sinai*: AmphD and CpxD = amphibole- and augite-bearing Neoproterozoic dikes from Wadi Feiran, Wadi El-Sheikh, and Gebel Minadir areas (Iacumin et al., 1998); D = Pan-African dikes, generations L1 and S2 from the Wadi Feiran area, (Friz-Töpfer, 1991). (10, 2)* = number of analyses used for calculation of average compositions: the first figure for major elements and Rb, Ba, Sr, Zr, Nb, Y; the second figure for REE, Hf, Ta, and Th.

TH2 (Stein et al., 1997) are typical trachydolerites rather than tholeiites. Considering this correction, a significant part of the TH1 suite can be correlated with our dike suite 3.

Suite 4 is distinct from suite 3 by its younger relative age and by being composed solely of mafic dikes. Suite 4 in Elat thus resembles other high-TiO_2 dolerite dike swarms that constitute the youngest dike generation throughout the northernmost Arabian–Nubian Shield (Friz-Töpfer, 1991; Iacumin et al., 1998; Kessel et al., 1998; Beyth and Heimann, 1999; Essawy and El-Metwally, 1999; Jarrar, 2001). The heavy alteration of suite 4 in Elat hampers reliable correlation by petrographic features and mobile element contents. The HFS element contents (Ti, Zr, and, particularly, Nb) of suite 4 trachydolerites are comparable to those of a spectacular NW-trending mafic dike swarm exposed in SW Sinai (Essawy and El-Metwally, 1999). However, suite 4 is less enriched in HFSE relative to the Amram dolerites that constitute the AB suite (alkaline basalt, formerly termed TH2) of Kessel et al. (1998; Table 2) and to the youngest dolerites in southern Jordan (Jarrar, 2001). Future age determinations may allow better distinction between different episodes of dolerite dike emplacement that forms the youngest magmatism in the crystalline basement of the ANS.

Judging by the available geochronological data, the time span between the first and last dike episodes was prolonged. The U-Pb age of 605 ± 5 Ma for the Yehoshafat granite that followed the first dike suite (Beeri, pers. comm.) and the $^{39}Ar/^{40}Ar$ age of 531 ± 4.6 Ma for the latest high-Ti dolerite dike in the Timna block (Beyth and Heiman, 1999) indicate that the formation of dike suites lasted for at least 70 My. This estimate is supported by Rb-Sr dating of Late Pan-African dikes in Sinai: the oldest age is about 590 Ma (Stern and Manton, 1987). The main dike episodes were divided in time by plutonic, volcanic, and sedimentation events (Table 1). In light of these data it is clear that dikes from different suites, despite their close association in space, were produced from different magma sources rather than from a single magma chamber.

In order to investigate the nature of magma sources and magma genesis, we focused on the mafic rocks from each dike suite, assuming that mafic magmas were derived from mantle sources.

Sources of magmas

Microdiorite and lamprophyre from suite 1 are medium- to high-K calc-alkaline rocks (Fig. 7). Phenocrysts of hornblende occur in both rock types along with plagioclase in the microdiorite. According to experimental data, early crystallization of amphibole in the absence of plagioclase points to high water content in the melt, about 4–6 wt% H_2O at a pressure of 2 kbar (Anderson, 1980 and references therein; Baker and Eggler, 1983; Sisson and Grove, 1993). Liquidus crystallization of both hornblende and plagioclase occurs at lower water contents (≤ 3 wt% H_2O, Sisson and Grove, 1993). These experimental constraints point to significant water enrichment of the lamprophyre and, to a lesser extent, diorite magmas.

The chemical composition of microdiorite (average composition, see Table 4) is shown on a MORB-normalized multi-element diagram (Fig. 12A). Enrichment in LILE (K, Rb, Ba, Th) relative to HFSE (Ta, Nb, P, Zr, Ti, Y, REE), clear negative Nb anomaly and weak Ti trough are typical of calc-alkaline subduction-related rocks from orogenic belts. Its strong incompatible element enrichment and steep REE patterns (La/Yb_N = 11; Fig. 12B, Table 4) are comparable to high-K and medium-K calc-alkaline volcanic rocks that are abundant at active continental margins (Gill, 1981; Gómez-Tuena and Carrasco-Núñez, 2000). The multi-element and REE patterns (Fig. 12A, B) of microdiorite fit in well with the composition of basalts from the classic Oligocene western Oaxaca province (Mexico) formed in a subduction-related environment (Martiny et al., 2000).

The position of lamprophyre in the MORB-normalized diagram is similar to that of microdiorite, but in comparison with typical calc-alkaline rocks they contain less LREE and MREE (Fig. 12B). The higher contents of MgO and FeO*, and lower SiO_2, Sr, and Zr in the lamprophyre compared to microdiorite (Fig. 7) suggest that the lamprophyre melt can be considered as parental for microdiorite. However, this assumption is inconsistent with the similar contents of CaO, TiO_2, K_2O, Rb, and HREE in the microdiorite and the lamprophyre (Table 4 and Figs. 7,8). In addition, such a model requires that the residual melt should be water-enriched compared to the parental magma, but the real situation is inverse. It is likely that although these rocks are related they are derived from slightly different sources.

Andesite porphyry dikes of suite 2 represent the onset of a new dike episode following the Yehoshafat alkaline granite emplacement. It is characterized by lower SiO_2, CaO, Ba, Sr, and LREE and higher MgO, TiO_2 and FeO^T relative to the suite 1 microdiorite (Figs. 11, 12B; Table 4). However, the pattern of andesite porphyry in the MORB-normalized diagram shows significant similarities to suite 1 microdiorite (Fig. 12A). The main mafic

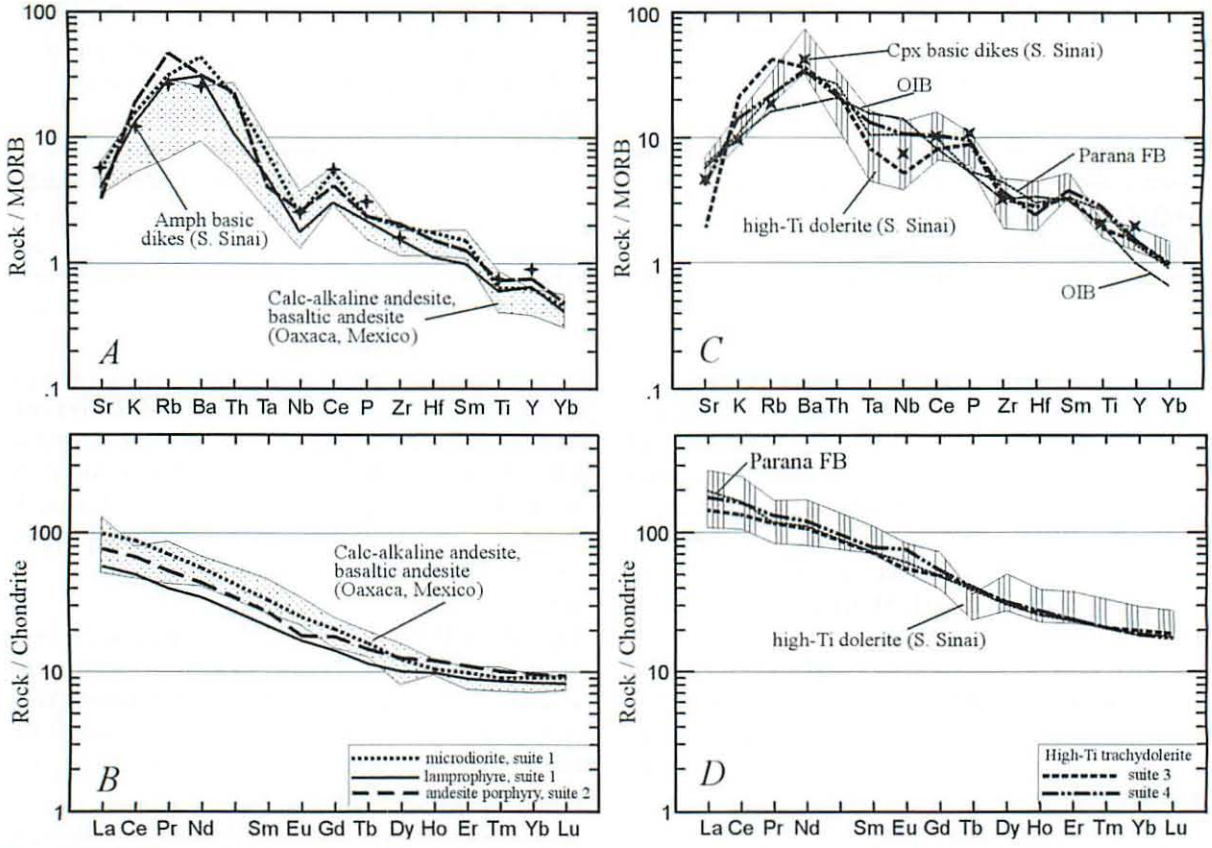

Fig. 12. MORB- and chondrite-normalized diagrams for basic rocks from the four successive dike suites (average compositions). Sources: Amph and Cpx basic dikes (S. Sinai)—Iacumin et al. (1998); high-Ti dolerite (S. Sinai)—Friz-Töpfer (1991); calc-alkaline basaltic andesite and andesite (Oaxaca, Mexico)—Martiny et al. (2000); Parana flood basalt (FB)—Thompson et al. (1983); OIB—Sun and McDonough (1989). MORB values after Pearce (1983).

mineral in the andesite porphyry is augite, which suggests that the magma was impoverished in H_2O. It follows that andesitic magmas from the first and second suites could have been derived from the same source: first melting of a wet mantle source that is rich in incompatible elements followed by melt extraction from the already drier, less enriched source.

Thus, the mafic magmas of the first and second dike suites were similar to those formed in a subduction-related setting. The negative spike in Nb and the trough in Ti could be caused either by retention of Nb- and Ti-bearing phases in the solid residue (Ryerson and Watson, 1987; McCulloch and Gamble, 1991; Maury et al., 1992; Iacumin et al., 1998), or by the effect of slab-derived fluid that defined zoning in mantle wedge (Stein et al., 1997). According to the model devised by Stein and coworkers, Nb is enriched only in the lower zones of the column. The source region for calc-alkaline magmas was located in the zone above the Nb concentration front in the central part of the fossilized wedge. The timing of dike injection of suites 1 and 2 far post-dated active subduction in the ANS. This suggests that the source region in the lithospheric mantle was only slightly modified after the former subduction event that had been completed more than 50 My before the first dike episode. A similar conclusion was drawn by other authors studying the Late Pan-African dikes in the Sinai Peninsula and Eastern Desert (Friz-Töpfer, 1991; Iacumin et al., 1998; Abu-El-Ela and Salem, 1999; Essawy and El-Metwally, 1999; Moghazi, 2003).

The high-Ti trachydolerite patterns (suites 3 and 4) are shown in MORB- and chondrite-normalized diagrams (Fig. 12C,D), along with patterns of Parana Flood Basalts and OIB used for comparison. Chemical characteristics of trachydolerites from both dike suites are rather similar and resemble those of OIB. However, almost total similarity is exhibited with Parana Flood Basalts, one of the most representative continental flood basalt provinces (Thompson et al., 1983).

Although processes defining the typical chemistry of flood basalts are still a subject of debate (e.g., Lightfood and Hawkesworth, 1988), all authors agree that their high-Ti and high-P abundances reflect derivation of basic magma from enriched mantle sources. Crustal contamination could not play an important role since the contents of Ti and P in crustal rocks are low (Rudnick and Fountain, 1995). It follows that K and Rb, as well as REE and other HFSE enrichments in dolerites (Tables 2 and 3), stemmed from an asthenospheric component, as suggested for giant Late Pan-African dike swarms from the Adrar des Iforas, Mali (Liégeois and Black, 1987). The asthenospheric effect could be combined with melting of the metasomatized mantle wedge (Stein et al., 1997).

The occurrence of Late Pan-African dike swarms is not limited to southern Israel. Similar dikes are abundant throughout the Sinai Peninsula and eastern desert of Egypt. Although the chronological sequence of dike episodes is not always sufficiently clear, the similarity in chemistry and petrography with dikes from the central Elat area allows one to compare their patterns in multi-element diagrams. In Fig. 12 compositions of amphibole-bearing andesite and basaltic andesite, pyroxene-bearing basalt, and basaltic trachyandesite (Iacumin et al., 1998), and high-Ti dolerite (Friz-Töpfer, 1991) from southern Sinai are shown. The average compositions of these rocks are given in Table 4 (for calculation of the average composition of the high-Ti dolerite we chose samples with Eu/Eu* ≤1 and SiO_2 ranging from 45 to 51 wt%). Almost entire overlap of dike rock compositions from southern Israel and southern Sinai is observed. This suggests that data on sequence, composition, petrography, and chemistry of dike swarms obtained in southern Israel are appropriate for Late Pan-African dikes of the Sinai Peninsula and adjacent areas.

CONCLUSIONS

1. In the central Elat area four successive Late Pan-African dike episodes are recognized. The dike episodes alternated with plutonic, volcanic, and sedimentary events, and formation of dikes lasted over a long period of about 70 My, from ~600 Ma to 530 Ma.
2. There is no correlation between the strike of the dikes and their age. This suggests that the stress field that controlled the dike swarm trends existed (or appeared) still at the earliest dike stage and did not markedly change during the whole period of dike formation.
3. Dike rock compositions systematically changed over time from calc-alkaline medium-K to high-K and shoshonitic series.
4. Although Late Pan-African dikes are postorogenic, generation of magmas during the formation of the first two suites occurred from mantle sources, which are characteristic of a subduction-related environment at an active continental margin.

ACKNOWLEDGMENTS

This study was supported by grants from the Ministry of National Infrastructure and Energy, Israel (#23–17–04) and from the Israel Science Foundation (#142/02). The authors are grateful to R. Shagam and V. Voznesensky for the fruitful collaboration and thoughtful comments. Recommendations given in a thorough review by Oded Navon enabled us to significantly improve the initial version of the paper.

REFERENCES

Abu-El-Ela, A.M., Salem, I.A. 1999. Petrological and geochemical studies on the dyke swarms of the Kadabora granite pluton, Eastern Desert, Egypt. Ann. Egypt Geol. Surv. 22: 47–63.

Agron, N., Bentor, Y.K. 1981. The volcanic massif of Biq'at Hayareah (Sinai-Negev), a case of potassium metasomatism. J. Geol. 89: 479–496.

Anderson, A.T. 1980. Significance of hornblende in calc-alkaline andesites and basalts. Am. Mineral. 65: 837–851.

Baer, G., Beyth, M., Reches, Z. 1993. The mechanics of dike emplacement into fractured basement rocks, Timna igneous complex, Israel. Isr. Geol. Soc. Annu. Mtg., p. 8.

Baker, D.R., Eggler, D.H. 1983. Fractionation paths of Atka (Aleutians) high-alumina basalts: constraints from phase relations. J. Volcanol. Geotherm. Res.18: 387–404.

Bentor, Y.K. 1985. The crust evolution of the Arabo-Nubian Massif with special reference to the Sinai Peninsula. Precambr. Res. 28: 1–74.

Bentor, Y.K., Eyal, M. 1987. The geology of southern Sinai, its implication for the evolution of the Arabo-Nubian Massif. Isr. Acad. Sci. Humanities, Jerusalem, 484 pp.

Beyth, M., Heimann, A. 1999. The youngest igneous event in the crystalline basement of the Arabian–Nubian Shield, Timna Igneous Complex. Isr. J. Earth Sci. 48: 113–120.

Druckman, Y., Weissbrod, T., Garfunkel, Z. 1993. Geological map of Israel, scale 1:100,000 (sheets 25 and 26 Elat). Geological Survey of Israel, Jerusalem.

El-Metwally, A.A. 1997. Sinai mafic and felsic dykes: geochemistry and emplacement model. Egypt J. Geol. 41/1: 357–386.

Essawy, M.A, El-Metwally, A.A. 1999. Petrogenesis of a high TiO_2 mafic dyke swarm from Southwest Sinai. J. Afric. Earth Sci. 29/3: 551–565.

Eyal, Y., Eyal, M. 1987. Mafic dyke swarms in the Arabo-Nubian Shield. Isr. J. Earth Sci. 36: 195–221.

Eyal, Y., Eyal, M., Kröner, A. 1991. Geochronology of the Elat Terrain metamorphic basement, and its implication for crustal evolution of the NE part of the Arabian–Nubian Shield. Isr. J. Earth Sci. 40: 5–16.

Eyal, M., Voznesensky, V., Bentor, Y. 1995. The geological map of the Katherina Ring Complex, 1:50,000. Isr. Geol. Soc. Annu. Mtg., p. 28.

Eyal, M., Litvinovsky, B.A., Katzir, Y., Zanvilevich, A.N. 2004. Neoproterozoic calc-alkaline, high-K, peraluminous Elat granite of southern Israel: geology, geochemistry and petrogenesis. J. Afric. Earth Sci. 40/3–4: 115–136.

Friz-Töpfer, A. 1991. Geochemical characterization of Pan-African dyke swarms in southern Sinai: from continental margin to intraplate magmatism. Precambr. Res. 49: 281–300.

Garfunkel, Z. 1999. History and paleogeography during the Pan-African orogen to stable platform transition: reappraisal of the evidence from the Elat area and the northern Arabian–Nubian Shield. Isr. J. Earth Sci. 48: 135–157.

Garfunkel, Z., Eyal, Y., Eyal, M., Weissbrod, T., Bakler, N., Shimron, A.E., Peltz, S., Gutkin, V., Bartov, Y., Drukman, Y., Rozenfeld, M., Sneh, A. 2000. Geological map of the Northern Gulf of Elat area, scale 1:100,000 (sheet 26 Elat). Geological Survey of Israel, Jerusalem.

Gass, I.G. 1982. Upper Proterozoic (Pan-African) calc-alkaline magmatism in North-eastern Africa and Arabia. In: Thorpe, R.S., ed. Andesites and related rocks. Chichester, UK, Wiley, pp. 595–609.

Genna, A., Nehlig, P., Le Goff, E., Gguerrot, Cc., Shanti, M. 2002. Proterozoic tectonism of the Arabian Shield. Precambr. Res. 117/1–2: 21–40.

Gill, G. 1981. Orogenic andesites and plate tectonics. Springer-Verlag, New York, 390 pp.

Gómez-Tuena, A., Carrasco-Núñez, G. 2000. Cerro Grande volcano: the evolution of a Miocene stratocone in the early Trans-Mexican Volcanic Belt. Tectonophysics 318: 249–280.

Greiling, R.O., Abdeen, M.M., Dardir, A.A., El Akhal, H., El Ramly, M.F., Kamal El Din, G.M., Osman, A.F., Rashwan, A.A., Rice, A.H.N., Sadek, M.F. 1994. A structural synthesis of the Proterozoic Arabian-Nubian Shield in Egypt. Geologische Rundschau 83: 484–501.

Gutkin, V., Eyal, Y. 1998. Geology and evolution of Precambrian rocks, Mt. Shelomo, Elat area. Isr. J. Earth Sci. 47/1: 1–18.

Iacumin, M., Mazaroli, A., El-Metwally, A.A., Piccirillo, E.M. 1998. Neoproterozoic dyke swarms from southern Sinai (Egypt): geochemistry and petrogenetic aspects. J. Afric. Earth Sci. 26: 49–64.

Jarrar, G. 2001. The youngest Neoproterozoic mafic dike suite in the Arabian Shield: mildly alkaline dolerites from South Jordan—their geochemistry and petrogenesis. Geol. Mag. 138: 309–323.

Katz, O., Avigad, D., Matthews, A., Heimann, A. 1998. Precambrian metamorphic evolution of the Arabian–Nubian shield in the Roded area, southern Israel. Isr. J. Earth Sci. 47/2: 93–110.

Kessel, R. 1995. The geochemistry of dykes and their host rocks from the latest stages of the Pan African orogeny, Amram and Elat massifs, southern Israel. M.Sc. thesis, Hebrew Univ., Jerusalem, 121 pp. (in Hebrew).

Kessel, R., Stein, M., Navon, O. 1998. Petrogenesis of late Neoproterozoic dikes in the northern Arabian-Nubian Shield. Implication for the origin of A-type granites. Precambr. Res. 92: 195–213.

Kröner, A., Greiling, R., Reischmann, T., Hussein, I.M., Stern, R.J., Durr, S., Krugger, J., Zimmer, M. 1987. Pan-African crustal evolution in the Nubian segment of north-eastern Africa. In: Kröner, A., ed. Proterozic lithospheric evolution. Am. Geophys. Union, Geodynamic Ser. 15: 235–257.

Le Maitre, R.W., ed. 1989. A classification of igneous rocks and glossary of terms. Blackwell Scientific Publ., Oxford, 193 pp.

Liégeois, J.-P., Black, R. 1987. Alkaline magmatism subsequent to collision in the Pan-African belt of the Adrar des Iforas. In: Fitton, J.G., Upton, B.G.J., eds. Alkaline igneous rocks. Geol. Soc. Spec. Publ., Vol. 30, pp. 381–401.

Lightfood, P., Hawkesworth, C. 1988. Origin of Deccan trap lavas: evidence from combined trace element and Sr-, Nd-, and Pb-isotope studies. Earth Planet. Sci. Lett. 91: 89–104.

Martiny, B., Martinez-Serrano, R.G., Morán-Zenteno, D.J., Masías-Romo, C., Ayuso, R.A. 2000. Stratigraphy, geochemistry and tectonic signisicance of the Oligocene magmatic rocks of western Oaxaca, southern Mexico. Tectonophysics 318: 71–978.

Maury, R.C., Defant, M.J., Joron, J.L. 1992. Metasomatism of the sub-arc mantle inferred from trace elements in Philippine xenoliths. Nature 360: 661–663.

McCulloch, M.T., Gamble, J.A. 1991. Geochemical and geodynamical constraints on subduction zone magmatism. Earth Planet. Sci. Lett. 102: 321–355.

Moghazi, A.M. 2003. Geochemistry and petrogenesis of a high-K calc-alkaline Dokhan Volcanic suite, South Safaga area, Egypt: the role of late Neoproterozoic crustal extension. Precambr. Res. 125/1–2: 161–178.

Mushkin, A., Navon, O., Halicz, L., Heimann, A., Woerner, G., Stein, M. 1999. Geology and geochronology of the Amram Massif rocks, southern Negev Desert, Israel. Isr. J. Earth Sci. 48: 179–193.

Mushkin, A., Navon, O., Halicz, L., Heimann, A., Stein, M. 2003. The petrogenesis of A-type magmas from the Amram Massif, southern Israel. J. Petrol. 44/5: 815–832.

Pearce, J.A. 1983. Role of sub-continental lithosphere in magma genesis at active continental margins. In: Hawkesworth, C.J., Norry, M.J., eds. Continental basalts and mantle xenoliths. Shiva Publishing Limited, Nantwich, UK, pp. 230–249.

Rickwood, P.C. 1989. Boundary lines within petrologic

diagrams which use oxides of major and minor elements. Lithos 22: 247–263.

Roobol, M.J., Ramsay, C.R., Jackson, N.J., Darbyshire, D.P.F. 1983. Late Proterozoic lavas of the Central Arabian Shield – evolution of an ancient volcanic arc system. J. Geol. Soc. London 140: 185–202.

Rudnick, R.L., Fountain, D.M. 1995. Nature and composition of the continental crust: a lower crustal perspective. Rev. Geophys. 33/3: 267–309.

Ryerson, F.J., Watson, E.B. 1987. Rutile saturation in magmas: implication from Ti-Nb-Ta depletion in island-arc basalts. Earth Planet. Sci. Lett. 86: 225–239.

Sisson, T.W., Grove, T.L. 1993. Experimental investigations of the role of H_2O in calc-alkaline differentiation and subduction zone magmatism. Contrib. Mineral. Petrol. 113: 143–166.

Stein, M., Navon, O., Kessel, R. 1997. Chromatographic metasomatism of the Arabian-Nubian lithosphere. Earth Planet. Sci. Lett. 152: 75–91.

Stern, R.J., Hedge, C.E. 1985. Geochronologic and isotopic constraints on Late Precambrian crustal evolution in the Eastern Desert of Egypt. Am. J. Sci. 285: 97–127.

Stern, R.J., Gottfried, D. 1986. Petrogenesis of the Late Precambrian (575–600 Ma) bimodal suite in Northeast Africa. Contrib. Mineral. Petrol. 92: 492–501.

Stern, R.J., Manton, W.I. 1987. Age of Feiran basement rocks, the northern Arabian-Nubian Shield. J. Geol. Soc. London 144: 569–575.

Stern, R.J., Sellers, G., Gottfried, D. 1988. Bimodal dike swarms in the north of the Eastern Desert of Egypt: significance for the origin of the Precambrian "A-type" granites in Northern Afro-Arabia. In: Greiling, R., El-Gaby, R., eds. The Pan-African belt of NE Africa and adjacent areas: tectonic evolution and economic aspects. Frieder, Vieweg & Sohn, Braunschweig, Germany, pp. 147–179.

Sun, S., McDonough, W.F. 1989. Chemical and isotopic systematics of oceanic basalts: implications for mantle compositions and processes. In: Saunders, A.D., Norry, M.J., eds. Magmatism in the ocean basins. Geol. Soc. Special Publ. 42: 313–345.

Thompson, R.N., Morrison, M.A., Diskin, A.P., Hendry, G.L. 1983. Continental flood basalts... arachnids rule OK? In: Hawkesworth, C.J., Norry, M.J., eds. Continental basalts and mantle xenoliths. Shiva Publishing Limited, Nantwich, UK, pp. 158–185.

Voznesensky, V. 1998. The Precambrian of Sinai on a 1:50,000 scale; a series of geological maps along the El-Tur-Mt. Sinai-Elat direction. Isr. Geol. Soc. Annu. Mtg., p. 108.

Wachendorf, H., Zachmann, D., Jarrar, G.H. 1985. The role of pressure in control of potassium, sodium, and copper concentration in hypabyssal intrusives as demonstrated in Late Precambrian dikes in southern Jordan. Precambr. Res. 30: 221–248.

Whalen, J.B., Currie, K.L., Chappel, B.W. 1987. A-type granites: geochemical characteristics, discrimination and petrogenesis. Contrib. Mineral. Petrol. 95: 407–419.

Winchester, J.A., Floyd, P.A. 1977. Geochemical discrimination of different magma series and their differentiation products using immobile elements. Chem. Geol. 70: 319–339.